Modelling carbon and water cycles in a beech forest Part I: model description and uncertainty analysis on modelled NEE

E. Dufrene, H. Davi, C. François, G. Le Maire, Valérie Le Dantec, A. Granier

DTD 5
ARTICLE IN PRESS

Available online at www.sciencedirect.com
SCIENCE DIRECT®

ELSEVIER

Ecological Modelling xxx (2005) xxx–xxx

ECOLOGICAL MODELLING

www.elsevier.com/locate/ecolmodel

Modelling carbon and water cycles in a beech forest Part I: Model description and uncertainty analysis on modelled NEE

E. Dufrêne[a], H. Davi[a,*], C. François[a], G. le Maire[a], V. Le Dantec[b], A. Granier[c]

[a] *Ecologie, Systématique et Evolution (ESE), CNRS and Université Paris Sud, Bât 362, 91405 Orsay, France*
[b] *Centre Etudes Spatiales de la BIOsphere (CESBIO), (CNES/CNRS/UPS), Toulouse, France*
[c] *Unité Ecophysiologie, INRA-Nancy, F-54280 Champenoux, France*

Received 24 March 2004; received in revised form 20 December 2004; accepted 3 January 2005

Abstract

A forest ecosystem model (CASTANEA) is developed with the aim to bridge the gap between soil–vegetation–atmosphere (SVAT) and growth models. A physiologically multi-layer process-based model is built, completed with a carbon allocation model and coupled with a soil model. CASTANEA describes canopy photosynthesis and transpiration, maintenance and growth respiration, seasonal development, partitioning of assimilates to leaves, stems, branches, coarse and fine roots, evapotranspiration, soil heterotrophic respiration, water and carbon balances of the soil. Net primary productivity (NPP) is calculated as the difference between gross photosynthesis and plant respiration. The net ecosystem exchange (NEE) between soil-plant system and atmosphere is calculated as the difference between gross photosynthesis and total respiration (soil + plants). The meteorological driving variables are global radiation, rainfall, wind speed, air humidity and temperature (either half-hourly or daily values). A complete description of the model parameterization is given for an eddy flux station in a beech stand (Hesse, France). A parametric sensitivity analysis is carried out to get a classification of the model parameters according to their effect on the NEE. To determine the key input parameters, a +10% or −10% bias is applied on each of the 150 parameters in order to estimate the effect on simulated NEE. Finally 17 parameters, linked to photosynthesis, vegetative respiration and soil water balance, appear to have a significant effect (more than 2.5%) on the NEE. An uncertainty analysis is then presented to evaluate the error on the annual and daily NEE outputs caused by uncertainties in these input parameters. Uncertainties on these parameters are estimated using data collected in situ. These uncertainties are used to create a set of 17,000 simulations, where the values of the 17 key parameters are randomly selected using gaussian random distributions. A mean uncertainty of 30% on the annual NEE is obtained. This uncertainty on the simulated daily NEE does not totally explain the discrepancies with the daily NEE measured by the eddy covariance technique (EC). Errors on daily measurements by EC technique and uncertainty on the modelling of several processes may partly explain the discrepancy between simulations and measurements.

Keywords: Model; Carbon; Water; Growth; Eddy fluxes; NEE; NPP; Soil; Beech forest; Uncertainty analysis; Sensitivity analysis

* Corresponding author. Present address: CESBIO UMR 5126 (CNRS-UPS-CNES-IRD), 18 Avenue Edouard Belin, bpi 2801F 31401 Toulouse, Cedex 9, France. Tel.: +33 5 61 55 85 97/6 79 87 64 11; fax: +33 5 61 55 85 00.
E-mail address: hendrik.davi@cesbio.cnes.fr (H. Davi).

0304-3800/$ – see front matter © 2005 Elsevier B.V. All rights reserved.
doi:10.1016/j.ecolmodel.2005.01.004

1. Introduction

Long-term accurate estimates of (i) *carbon and water fluxes* between forest ecosystems and the atmosphere and (ii) *carbon storage* in trees and soil, are crucial to assess the role of forested areas in the global carbon cycle and in the continental water balance.

During the last century, several types of forest models have been developed with different objectives. Among the oldest, the empirical "*forestry*" models (Schober, 1975; Dhôte, 1990, 1991), with a time step of one year or more, predict stem growth without considering seasonal and inter-annual climatic changes. These models use empirical rules based on large data sets from field plots. They are able to reproduce tree growth over a century, according to forest management, age of stocking assuming no change in climate trend. However, climate change probably explains the increasing trend in radial growth (Becker et al., 1994) and in tree height (Dhôte and Hervé, 2000).

During the last two decades, several biophysical carbon/water fluxes models have been developed, considering the canopy as a single layer (i.e. "big-leaf"), a multi-layer or a three dimensional volume (Wang and Jarvis, 1990; Aber and Federer, 1992; Amthor, 1994; Baldocchi and Harley, 1995; De Pury and Farquhar, 1997). They assess mass and energy exchange between the canopy and the atmosphere by coupling the fluxes of carbon dioxide and water vapour. The leaf physiologically based photosynthesis model by Farquhar et al. (1980), linked with a stomatal conductance model (Jarvis, 1976; Ball et al., 1987; Collatz et al., 1991) provides a theoretical framework for spatially integrating fluxes from leaf to canopy level. These process-based models integrate accurately the canopy functioning over time from seconds to days (Caldwell et al., 1986; Baldocchi, 1992; Leuning et al., 1995; Williams et al., 1996; Wang and Leuning, 1998). They are not designed, however, to predict the seasonal and inter-annual variations of tree growth and stand biomass increment. *Forest growth* models, based on ecological and biogeochemical principles, focus on how carbon and water fluxes vary from daily to annual and decadal time scales. They are able to predict changes in plant carbon pools (i.e. organs) by understanding there respective size and turnover time (Mohren, 1987; McMurtrie et al., 1990). Some of these models consider litter and soil mineralization processes with the aim to predict soil organic matter dynamics (Running and Coughlan, 1988; Korol et al., 1991; Running and Hunt, 1993; Hoffmann, 1995; Bossel, 1996). However, they tend to ignore the effects of microclimate spatial variability within the plant canopy and, as they generally use a daily time step, they need empirical (i.e. not physiologically based) leaf and canopy photosynthesis sub-models. As hydrologic processes control drought effect on photosynthesis (Schulze, 1986) soil carbon and nitrogen dynamics (Parton et al., 1987), some of these models also couple the carbon budget with a model simulating the water cycle. The rainfall reaching the ground is shared out into soil evaporation, transpiration, interception, infiltration or runoff. According to the application domain, the hydrology models are more or less sophisticated. For example, the evapotranspiration can be calculated as function of a potential evaporation (Kim et al., 1996) or estimated following Monteith (1965) or Shuttleworth and Wallace (1985). The soil can be divided into numerous layers (Braud et al., 1995) or parameterized into one or several buckets (Eagleson, 1978). Nevertheless, detailed SVAT models are difficult to use for the investigation of the spatial and temporal variability of land surface fluxes. The large number of parameters they involve requires detailed field studies and experimentation to derive parameter estimates (Boulet et al., 2000). Simple water balance models using simple soil and stand parameters and basic climatic data are often sufficient to predict temporal variation in soil water content (Granier et al., 1999).

In this paper we focus on the complete description of a model simulating carbon, water and energy fluxes and we precisely describe the parameterization in the case of a beech forest stand (Hesse Euroflux site, France). A precise description of the CASTANEA structure and parameterization is given to account for the complexity and the large number of variables and parameters of this physiologically multi-layer process-based model. An effort concerning the parameterization has been done to have confidence in the model validation at eddy flux stations. Given the large number of input parameters, a sensitivity study, to determine the key parameters and their effect on the simulated output variables (uncertainty analysis), is presented. The uncertainty on the daily and annual simulated net ecosystem exchange (NEE) is then estimated using Monte-Carlo simulations.

2. Model description

2.1. General description

CASTANEA is a physiologically process-based model aiming at predicting the carbon and the water balances of an even-aged monospecific forest stand. Flux densities variables concerning CO_2, and H_2O are simulated and allow the calculation of the state variables, i.e. water and carbon contents.

Light interception and photosynthesis submodels are implemented in CASTANEA by using a multilayer canopy description. On the other hand, growth and allocation submodels, are treated using six compartments. Five compartments correspond to the main organs (see Fig. 1), while the last one, without explicit location, corresponds to the carbohydrate storage in the whole tree. One averaged tree is considered as representative of the whole stand (i.e the variability between trees is not taken into account). The soil water balance is simulated

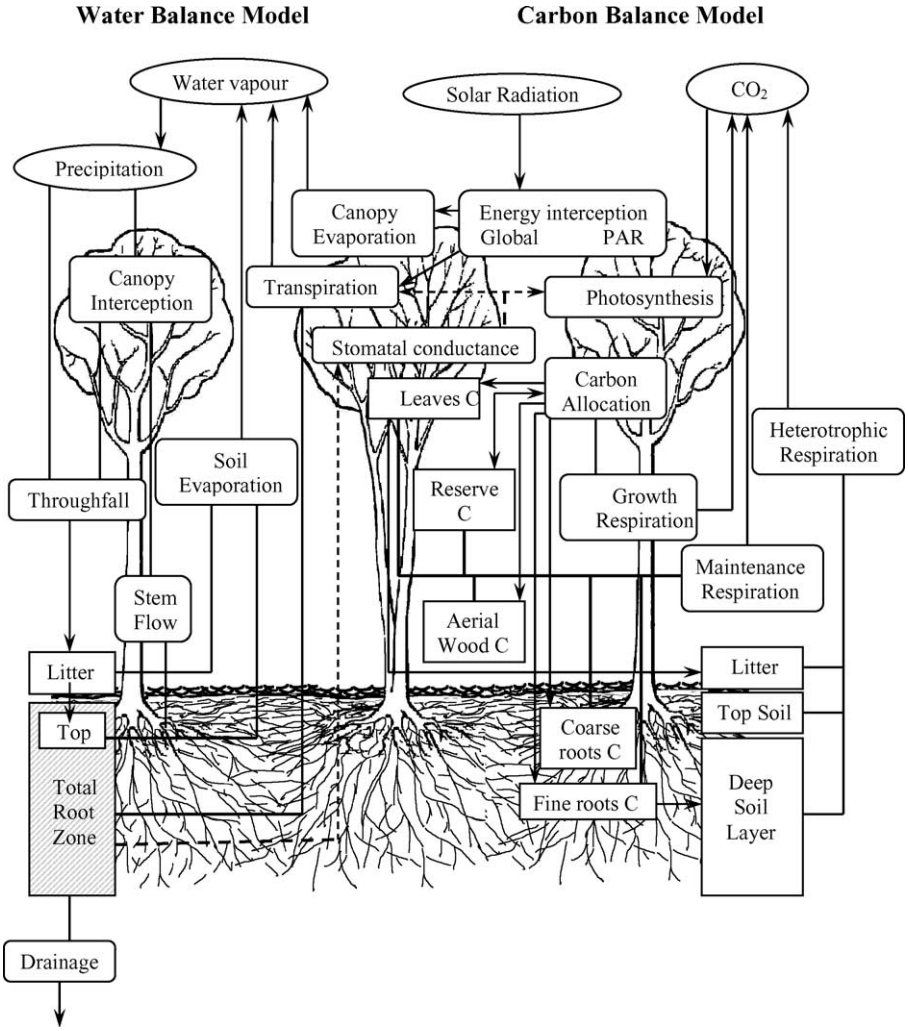

Fig. 1. Flow diagram for both water (left) and carbon (right) sub-models. Right angle boxes are state variables (C and H_2O), rounded angle boxes are flow variables (C and H_2O) and elliptic boxes are forcing meteorological variables. Each arrow corresponds to a water or carbon flow from one compartment to the next one. Dotted arrows correspond to (i) the influence of soil water content on stomatal opening and (ii) the stomatal control of both transpiration and photosynthesis.

with a bucket model including three layers. The soil organic carbon (SOC) model is similar to Parton's et al. (1987) approach except that two soil layers are considered (instead of one). Two time steps, half-hourly and daily, are used in the model. Most variables involving fluxes are simulated half-hourly; all state variables plus growth and phenology are daily simulated. Input meteorological driving variables can be either half-hourly or daily. If only daily values are available, the diurnal course (half-hourly values) of weather variables is generated according to the approach proposed by McMurtrie et al. (1990).

2.2. Radiation interception

The canopy is assumed to be horizontally homogeneous and vertically subdivided into a variable number of layers (i.e. multi-layer canopy model). Each layer contains the same amount of leaf area (typically less than $0.1\,m^2\,m^{-2}$). For each layer, the leaf inclination distribution function (LIDF) is represented through an ellipsoidal function (Campbell, 1986), discretized in eighteen steps between 0° and 90° and the same average leaf angle is assumed for all canopy layers.

Three different radiative balances are performed, in the PAR (400–700 nm), in the NIR (700–2500 nm), and in the thermal infrared. In the PAR and global regions, incident light is split into direct and sky diffuse radiation using equations given by Spitters (1986) and Spitters et al. (1986). In the thermal infrared, the diffuse atmospheric radiation is computed from air temperature according to Idso (1981).

2.2.1. Radiative balance in the thermal infrared

In the thermal infrared the radiative balance coefficients are based on the general formalism given in François (2002) (hereafter referred to as FR02). The soil and leaf emissivity are assumed to be constant, equal to 0.97. The canopy and the surface soil temperature are calculated iteratively by closing the energy budget (see later). The interception coefficient is computed according to Goudriaan (1977). The soil-vegetation radiative balance coefficients are written according to the third model (MOD3) presented in FR02, including multiple scattering parameterization (Eqs. (11), (14), (16) and (17) in FR02) and adapted for diffuse radiation. These coefficients are τ_v, ρ_v (resp. canopy simple transmittance and reflectance), τ_t, ρ_t, (resp. multiple scattering canopy transmittance and reflectance), and ω_t and ε_t (resp. multiple scattering vegetation emissivity and canopy emissivity). The details of the expression for the coefficients and the expression for the radiative transfer balance are given in Appendix A.

2.2.2. Radiative transfer in the PAR and NIR waveband

The leaf reflectance and transmittance in the PAR (resp. the NIR) are assumed to be constant inside the canopy (see Table 1). The diffuse and direct absorbed PAR ($aPAR_d$ and $aPAR_s$) and the absorbed NIR are computed for each layer. The radiation extinction and diffusion are based on the SAIL model (Verhoef, 1984, 1985). The SAIL model is used to compute the five elementary reflectances (ρ) and transmittances (τ) for an elementary layer: ρ_{dd}, ρ_{sd}, τ_{dd}, τ_{sd}, τ_{ss} (where the subscript s stands for direct radiation, and d for the diffuse radiation; first position is for incident radiation and second for transmitted or scaterred radiation). The calculation of the multi-layer radiative balance is described in Appendix B. The soil is treated as a particular layer, with no transmittance and having a reflectance based on the surface wetness

Finally, a classical radiative balance equation is written combining the radiative balance in the PAR, NIR and thermal infrared region, to calculate the net radiation Rn_{veg} for the vegetation and Rn_{soil} for the soil. The leaf (T_{leaf}) and soil temperatures (T_{soil}), are then computed by solving iteratively the equations of the energy balance.

Canopy clumping is taken into account in the model by using a clumping factor (agreg) in the radiative transfer model. For each leaf layer this factor reduces the leaf area used in the SAIL sub-model for radiation intercepting. The way to estimate the clumping factor is specified in §3-in situ measurements.

2.3. Leaf photosynthesis and stomatal conductance

The leaf photosynthesis (A) is represented using a C_3 plants biochemical process-based model, according to Farquhar et al. (1980). The CO_2 demand is determined as the minimum between Rubisco carboxylation and RuBP regeneration, while CO_2 supply depends on the difference in CO_2 concentration between the air outside the leaf and the carboxylation sites.

Table 1
List of parameters

Symbol	Description	Units	Value	Reference
Radiation and canopy structure				
Long	Longitude	Degree	48.66	
Lat	Latitude	Degree	−7.08	
ρ_{PAR}	Leaf reflectance for PAR radiation	Dimensionless	0.05	mean typical value (François, pers. com.).
τ_{PAR}	Leaf transmittance for PAR radiation	Dimensionless	0.11	mean typical value (François, pers. com.).
ρ_{NIR}	Leaf reflectance for NIR radiation	Dimensionless	0.32	mean typical value (François, pers. com.).
τ_{NIR}	Leaf transmittance for NIR radiation	Dimensionless	0.26	mean typical value (François, pers. com.).
$\rho_{soildNIR}$	Dry soil reflectance for NIR radiation	Dimensionless	0.10	Nagler et al. (2000)
$\rho_{soilwNIR}$	Wet soil reflectance for NIR radiation	Dimensionless	0.28	Nagler et al. (2000)
α_L	Average leaf angle inside the canopy	Radians	0.42	Planchais and Pontailler, (1999)
LMA_{sunmax}	Maximum sunlit leaf mass per area	$g_{dm}\ m^{-2}$	101	Montpied (pers. com.)
k_{LMA}	Leaf mass per area decrease coefficient	Dimensionless	0.187	Montpied (pers. com.)
WAI	Wood area index	$m_{wood}^2\ m_{soil}^{-2}$	0.75	Damesin et al. (2002)
L_{max}	Maximum leaf area index	$m_{leaf}^2\ m_{soil}^{-2}$	5.6	Bréda (pers. com.)
Agreg	Clumping factor		0.79	Soudani (pers. com., data 2000)
Carbon				
Leaf and canopy photosynthesis				
C_a	Atmospheric carbon dioxide concentration	$\mu mol\ CO_2\ mol\ air^{-1}$	370	Granier (pers. com.)
α_{Na}	Dependency between V_{Cmax} and leaf nitrogen density	$\mu mol\ CO_2\ g_N^{-1}\ s^{-1}$	20	Liozon et al. (2000)
β	Ratio between V_{Cmax} and V_{Jmax}	Dimensionless	2.1	Liozon et al. (2000)
α	Quantum yield	mol electrons (mol quanta)$^{-1}$	0.292	Ehleringer and Björkman (1977)
θ	Curvature of the quantum response of the electron transport rate	Dimensionless	0.1	fixed
g_{bCO_2}	Leaf boundary layer conductance	$mol\ CO_2\ m^{-2}\ s^{-1}$	1	calculated from leaf size
g_0	Leaf cuticular conductance	$mol\ H_2O\ m^{-2}\ s{-}^{1}$	0.001	fixed
g_{1max}	Slope of the Ball relationship (maximum value)	Dimensionless	11.8	Medlyn et al. (2001)
g_{1min}	Slope of the Ball relationship (minimum value)	Dimensionless	0.001	fixed
Maintenance respiration				
$Q_{10\ stem}$	Temperature effect for stem wood	Dimensionless	1.7	Damesin et al. (2002)
$Q_{10\ branches}$	Temperature effect for branches	Dimensionless	2.8	Damesin et al. (2002)
$Q_{10\ coarse\ roots}$	Temperature effect for coarse roots	Dimensionless	1.7	fixed
$Q_{10\ fine\ roots}$	Temperature effect for fine roots	Dimensionless	2.2	Epron et al. (2001)
$Q_{10\ leaves}$	Temperature effect for leaves	Dimensionless	2.1	Vose and Bolstad (1999)
T_{MR}	Base temperature for maintenance respiration	°C	15	Damesin et al. (2002)
$N_{mleaves}$	Leaves nitrogen content	$mg_N\ g_{dm}$	24.2	Montpied (pers. com.)
$N_{mbranches}$	Branch nitrogen content	$mg_N\ g_{dm}$	5.50	Ceschia et al. (2002)
$N_{mtrunks}$	Trunk nitrogen content	$mg_N\ g_{dm}$	1.20	Ceschia et al. (2002)
$N_{mcoarseroots}$	Coarse roots nitrogen content	$mg_N\ g_{dm}$	1.20	fixed
$N_{mfineroots}$	Fine roots nitrogen content	$mg_N\ g_{dm}$	9.90	Van Praag et al. (1988)
MRN	Nitrogen dependency for all organs	$mol\ CO_2\ g_N^{-1}\ h^{-1}$	5.5×10^{-4}	Ryan (1991)
$P_{leaf\ inhib}$	Inhibition of leaf respiration at light	Dimensionless	0.62	Villar et al. (1995)
Leaf phenology: budburst, growth and fall				
N_{Start1}	The date of onset of rest	Julian day	25	Dufrêne (unpublished data)
T_2	Base temperature for forcing budburst	°C	1	Dufrêne (unpublished data)
F_{critBB}	Critical value of state of forcing (from quiescence to active period)	°C	580	Dufrêne (unpublished data)

Table 1 (*Continued*)

Symbol	Description	Units	Value	Reference
T_3	Base temperature for leaf growth	°C	0	Fixed
LA_{max}	Maximum area reached by leaf (in average)	m^2	0.002	Le Dantec et al. (2000)
N_{Start2}	The date of onset of ageing	Julian day	213	Fixed
T_4	Base temperature for forcing leaf fall	°C	20	Fixed
$F_{critLfall}$	Critical value of state of forcing (from N_{Start2} to leaf fall period)	°C	225	calibrated
P_{fall}	Leaf ageing parameter	Dimensionless	0.4	calibrated
$F_{critLMA}$	Critical value of state of forcing (from leaf development to leaf maturity)	°C	424	estimated (see text)
Allocation				
$AG_{aerialwood}$	Aerial wood allocation coefficient	Dimensionless	0.51	calculated as a difference
$AG_{coarseroots}$	Coarse roots allocation coefficient	Dimensionless	0.10	ratio to aerial (0.2)
$AG_{fineroots}$	Fine roots allocation coefficient	Dimensionless	0.22	estimated
$AG_{storage}$	Storage allocation coefficient	Dimensionless	0.18	Barbaroux (2002)
$TO_{fineroots}$	Fine roots turn over	$jour^{-1}$	1/365	Bauhus and Bartsch (1996)
P_{branch}	Proportion of branches among aerial wood	Dimensionless	0.125	Damesin et al. (2002)
$P_{alive\ branch}$	Proportion of living cells in branches	Dimensionless	0.37	Ceschia et al. (2002)
$P_{alive\ trunk}$	Proportion of living cells in trunks	Dimensionless	0.21	Ceschia et al. (2002)
Growth respiration				
CR_{leaves}	Leaf construction cost	$gC\ gC^{-1}{}_{organ}$	1.20	Niinemets (1999)
CR_{wood}	Wood construction cost	$gC\ gC^{-1}{}_{organ}$	1.38	Damesin et al. (2002)
$CR_{fine\ roots}$	Fine roots construction cost	$gC\ gC^{-1}{}_{organ}$	1.28	Ågren and Axelsson (1980)
Heterotrophic (soil) respiration				
$Rmob_{leaf}$	Fraction of *N* not remobilized before leaf dead	Dimensionless	0.6	Montpied (pers. com.)
$Rmob_{fineroots}$	Fraction of *N* not remobilized before fine root dead	Dimensionless	1.0	fixed
Lig_{leaf}	Lignin concentration in leaves	$mg\ g_{dm}{}^{-1}$	196	Le Dantec (2000)
$Lig_{fineroot}$	Lignin concentration in fine roots	$mg\ g_{dm}{}^{-1}$	229	Chen et al. (2002)
T_b (top)	Base temperature for decomposition rate in the top soil layer	°C	35.0	Parton et al. (1987)
h (top)	Parameter for temperature effect on DR in the top soil layer	Dimensionless	2.63	Parton et al. (1987)
T_b (deep)	Base temperature for decomposition rate in the deep soil layer	°C	25.0	Parton et al. (1987)
h (deep)	Parameter for temperature effect on DR in the deep soil layer	Dimensionless	4.9	Parton et al. (1987)
T_B (surface)	Base temperature for decomposition rate at the surface	°C	25.0	Le Dantec (2000), Käärik (1974), Rayner and Boddy (1988)
h (surface)	Parameter for temperature effect on DR at the surface	Dimensionless	4.9	Le Dantec (2000), Dommergues and Mangenot (1970), Käärik (1974), Rayner and Boddy (1988)
T_{silt} (top)	Fraction of silt in the top soil layer	Dimensionless	0.68	Farque (1997)
T_{clay} (top)	Fraction of clay in the top soil layer	Dimensionless	0.26	Farque (1997)
T_{sand} (top)	Fraction of sand in the top soil layer	Dimensionless	0.06	Farque (1997)
T_{silt} (deep)	Fraction of silt in the deep soil layer	Dimensionless	0.62	Farque (1997)
T_{clay} (deep)	Fraction of clay in the deep soil layer	Dimensionless	0.32	Farque (1997)
T_{sand} (deep)	Fraction of sand in the deep soil layer	Dimensionless	0.06	Farque (1997)
K_{LLst}	Maximum decomposition rate for the surface structural litter pool	Day^{-1}	1.07×10^{-2}	Waelbroeck (1995)
K_{LLm}	Maximum decomposition rate for the surface metabolic litter pool	Day^{-1}	4.05×10^{-2}	Waelbroeck (1995)

Table 1 (*Continued*)

Symbol	Description	Units	Value	Reference
K_{RLst} (l)	Maximum decomposition rate for both top and deep structural litter pools	Day^{-1}	$1.34\ 10^{-2}$	Waelbroeck (1995)
K_{RLm} (l)	Maximum decomposition rate for both top and deep metabolic litter pools	Day^{-1}	5.07×10^{-2}	Waelbroeck (1995)
K_{Ca} (lit)	Maximum decomposition rate for the surface active microbial C pool	Day^{-1}	1.64×10^{-2}	Waelbroeck (1995)
K_{Ca} (l)	Maximum decomposition rate for both top and deep active microbial C pools	Day^{-1}	2.00×10^{-2}	Waelbroeck (1995)
K_{Cs} (l)	Maximum decomposition rate for both top and deep slow C pools	Day^{-1}	5.48×10^{-4}	Waelbroeck (1995)
K_{Cp} (l)	Maximum decomposition rate for both top and deep passive C pools	Day^{-1}	1.23×10^{-5}	Waelbroeck (1995)
Water				
Rainfall interception model constants				
RA_{bark}	Water storage capacity per unit of bark area	$mm\ H_2O\ m^{-2}$	0.30	estimated
RA_{leaf}	Water storage capacity per unit of leaf area	$mm\ H_2O\ m^{-2}$	0.20	Nizinski and Saugier (1988)
C_{ia}	Interception slope	Dimensionless	0.85	calculated
C_{ib}	Interception intercept	$m^2\ m^{-2}$	1.9	calculated
$PROP_{EC}$	Allocation between stemflow and throughfall	Dimensionless	0.35	calibrated
Soil water balance				
$RW_{lit\ fc}$	Litter water capacity storage	mm	1.7	Fixed
g_{solmax}	Maximum soil water vapour conductance	$m\ s^{-1}$	1/800	Kelliher et al. (1986)
g_{solmin}	Minimum soil water vapour conductance	$m\ s^{-1}$	1/12900	Schaap et al. (1997)
H_{top}	Height of top soil layer	mm	300	fixed
H_{soil}	Height of total soil root zone	mm	1600	Granier et al. (2000b)
θ_{fctop}	Top soil volumetric humidity at field capacity	$cm^3\ cm^{-3}$	0.373	Estimated*
θ_{fcsoil}	Soil volumetric humidity at field capacity	$cm^3\ cm^{-3}$	0.349	Granier et al. (2000b)
$\theta_{wilttop}$	Top soil volumetric humidity at wilting point	$cm^3\ cm^{-3}$	0.166	Estimated*
$\theta_{wiltsoil}$	Soil volumetric humidity at wilting point	$cm^3\ cm^{-3}$	0.25	Granier et al. (2000b)
$Pclay_{soil}$	Fraction of clay (total soil)	Dimensionless	0.279	Granier et al. (2000b)
prac	Proportion of fine roots in top soil layer	Dimensionless	0.63	Quentin et al. (2001)
S_{Stress}	Soil water stress threshold	Dimensionless	0.4	Black (1979), Dufrêne et al. (1992)

* Estimated from vertical profiles of soil water content (Granier et al., 2000).

Three main Eqs. (1), (2), (4) determine the assimilation rate (A):

First, the carbon dioxide demand Eq. (1) writes:

$$A = \mathrm{Vc} - \mathrm{Rd} \tag{1}$$

where Vc is the carboxylation rate and Rd the dark respiration during the day. Rd is calculated assuming a light inhibition phenomenon (see respiration module).

Second, the carbon dioxide supply Eq. (2) is similar to the Ohm's law in electricity where stomata conductance for carbon dioxide ($g_{s_{CO_2}}$) acts like an inverse of a resistance, while the gradient of CO_2 between the evaporative site (C_i) and the leaf surface (C_s) acts like a potential difference.

$$A = g_{s_{CO_2}} \times (C_s - C_i) \tag{2}$$

C_s depends on atmospheric CO_2 (Ca), on A and on the leaf boundary layer conductance ($g_{b_{CO_2}}$)

$$A = g_{b_{CO_2}}(C_a - C_s) \Leftrightarrow C_s = \frac{C_a - A}{g_{b_{CO_2}}} \tag{3}$$

Third, the carbon dioxide control Eq. (4), which allows the stomatal conductance calculation according to Ball et al. (1987):

$$g_{s_{H_2O}} = \frac{g_0 + g_1 \times A \times \mathrm{RH}}{C_s} \tag{4}$$

where g_1 depends on soil water stress (see Eq. (55)), g_0 corresponds to cuticular conductance of the leaf and RH is the relative humidity in the surrounding air. Stomatal conductance for water $g_{s_{H_2O}}$ is proportionnal

to $g_{s_{CO_2}}$ according to the molecular properties of water vapour and carbon dioxide.

The equations system (1), (2) and (4) is solved using an analytical solution proposed by Baldocchi (1994) to calculate A, g_s and C_i.

The carboxylation rate (V_c) is limited either by RUBISCO activity (W_c) at low C_i or by electron transport rate (W_j) at higher C_i. Note that we have neglected the gradual transition from electron transport to Rubisco limitation (Kirschbaum and Farquhar, 1984; Collatz et al., 1991) which have very small effect, as only a small fraction of leaves are near the transition to light saturation (De Pury and Farquhar, 1997).

2.3.1. Effect of temperature on photosynthesis

The biochemical basis of the temperature dependence of photosynthesis has been included in the model following Nolan and Smillie (1976) for electron transport rate (V_{jmax}), Long (1991) for the carbon dioxide (C_i) and oxygen (O_i) concentrations at the evaporative sites, and Bernacchi et al. (2001) for all others.

2.3.2. Leaf nitrogen effect on photosynthesis

Leaf nitrogen effect on photosynthesis is taken into account assuming a linear relationship between the maximal carboxylation rate (V_{cmax}) and leaf nitrogen content per unit area N_a (constant along the leafy season, see Table 1), and a fixed ratio β between V_{cmax} and the potential rate of electron flow (V_{jmax}) (Wullschleger, 1993).

$$V_{cmax} = \alpha_{N_a} N_a \tag{5}$$

$$V_{jmax} = V_{cmax} \times \beta \tag{6}$$

2.4. Canopy photosynthesis

The leaf mass per area profile (LMA_L) is simulated using the following equation:

$$LMA_L = LMA_{sun} \exp(-k_{LMA} L) \tag{7}$$

where LMA_{sun} is the leaf mass per area for sun leaves at the top of the canopy, k_{LMA} is an exponential decrease coefficient, and L the leaf area index above the considered level inside the canopy. LMA_{sun} varies during leaf growth to reach a maximal value LMA_{Sunmax} (see Eq. (21)).

Leaf nitrogen concentration (per mass) $N_{mleaves}$ ($g_N\, g_{dm}{}^{-1}$) is assumed to be constant inside the canopy despite the fact that a slight increase is generally measured from the top to the bottom. Leaf nitrogen per unit leaf area N_a ($g_N\, m^{-2}{}_{leaf}$) is then calculated for each layer:

$$N_{a_L} = LMA_L \times N_{mleaves} \tag{8}$$

Photosynthesis is calculated layer per layer (typically less than $0.1\, m^2\, m^{-2}$), on sunlit (leaf area intercepting diffuse and direct PAR) and shaded (leaf area intercepting diffuse PAR only) foliage separately. Both contributions are summed and photosynthesis is finally summed for all layers over the canopy.

2.5. Phenology

All phenological events and growth are calculated on a daily time step. The phenological events (budburst, full leaf area development, full leaf maturity, start of leaf yellowing, complete canopy yellowing) depend on day-degrees and day duration. Leaf fall is assumed to occur simultaneously with senescence (i.e. yellowing). The phenology model has been calibrated in an additional site (Fontainebleau forest, near Paris), independent of the validation data set (see §3-in situ measurements).

2.5.1. Budburst

Budburst is simulated following the Eq. (9)–(11):

$$R_{frcBB} = \left\{ \begin{array}{llll} T & \text{if } T > T_2 & \text{and} & N > N_{start1} \\ 0 & \text{if } T \leq T_2 & \text{or} & N < N_{start1} \end{array} \right\} \tag{9}$$

where R_{frcBB} is the rate of forcing for bud break, T the mean daily temperature, T_2 the base temperature, N the day of year and N_{START1} the date of onset of rest.

$$S_{frcBB} = \sum_{N_{START1}}^{N} R_{frcBB} \qquad \text{if} \qquad S_{frcBB} < F_{critBB} \tag{10}$$

$$N_{BB} = N \quad \text{if} \qquad S_{frcBB} = F_{critBB} \tag{11}$$

with S_{frcBB} the state of forcing, F_{critBB} the critical value of state of forcing for the transition from quiescence to the active period and N_{BB} the day when bud break occurred.

2.5.2. Leaf area development

Leaf area development is then computed following the Eqs. (12)–(14):

$$S_{\mathrm{frcLA}} = \sum_{N_{\mathrm{BB}}}^{N_{\mathrm{LAmax}}} T \qquad \text{if} \qquad T > T_3 \tag{12}$$

$$\frac{\mathrm{dLA}}{\mathrm{d}t} = \begin{Bmatrix} (\mathrm{LA_{max}} \times T)/\mathrm{S_{frcLA}} & \text{if} & \mathrm{LA} < \mathrm{LA_{max}} \\ 0 & \text{if} & \mathrm{LA} = \mathrm{LA_{max}} \end{Bmatrix} \tag{13}$$

$$\mathrm{LN} = \frac{L_{\max}}{\mathrm{LA_{max}}} \tag{14}$$

$$L = \mathrm{LA} \times \mathrm{LN} \tag{15}$$

where S_{frcLA} is the state of forcing for leaf growth, T_3 the base temperature for leaf growth, LA the mean area per leaf for the day considered, $\mathrm{LA_{max}}$ the maximum area per leaf, L the leaf area index, $L_{\max}$ the maximum leaf area index, N_{LAmax} the day when L reaches $L_{\max}$ and LN the number of leaves in the canopy. Note that $\mathrm{LA_{max}}$ and LN are input parameters, consequently the maximum LAI ($L_{\max}$) is forced according to the year and site.

2.5.3. Leaf fall (i.e. yellowing)

Finally, in the same way the yellowing and the leaf fall are simulated (Eq. (16)–(19)):

$$R_{\mathrm{frcfall}} = \begin{Bmatrix} T_4 - T & \text{if} & T > T_4 & \text{and} & N > N_{\mathrm{start2}} \\ 0 & \text{if} & T \geq T_4 & \text{or} & N < N_{\mathrm{start2}} \end{Bmatrix} \tag{16}$$

with R_{frcLfall} the rate of forcing for leaf fall, T_4 the base temperature and N_{Start2} the date of onset of leaf ageing.

$$S_{\mathrm{frcLfall}} = \sum_{N_{\mathrm{start2}}}^{N} R_{\mathrm{frcLfall}} \qquad \text{if} \qquad S_{\mathrm{frcLfall}} < F_{\mathrm{critLfall}} \tag{17}$$

$$N_{\mathrm{Lfall}} = N \qquad \text{if} \qquad S_{\mathrm{frcLfall}} = F_{\mathrm{critLfall}} \tag{18}$$

with S_{frcLfall} the state of forcing, $F_{\mathrm{critLfall}}$ the critical value of state of forcing for the transition from full leaf development to the leaf fall period and N_{Lfall} the day when leaf fall started.

$$\frac{\mathrm{d}L}{\mathrm{d}t} = \begin{Bmatrix} L_{(N-1)}\{[(\mathrm{Dl}_N - \mathrm{Dl_{min}})/ \\ \quad (\mathrm{Dl_{NLfall}} - \mathrm{Dl_{min}})]^{\mathrm{Pfall}} - 1\} & \text{if } N > N_{\mathrm{Lfall}} \\ 0 & \text{if } L = 0 \end{Bmatrix} \tag{19}$$

with $L_{(N-1)}$ the leaf area index of the previous day, $\mathrm{Dl_N}$ the day duration (min), $\mathrm{Dl_{min}}$ the shortest day duration of the year and $\mathrm{Dl_{NLfall}}$ the duration of the day when leaf started to fall. P_{fall} is an empirical coefficient.

2.6. Allocation

Allocation of assimilates (daily time step) is based on constant coefficients coupled with a system of priorities varying along the year according to the phenological stage. The use of assimilates for maintenance respiration has priority over growth and storage allocation all over the year.

For temperate deciduous forest, the year can be divided into three periods:

(1) from budburst to maximum leaf maturity: sinks are maintenance respiration and leaves formation. The carbon previously stored is used as a source in addition to gross photosynthesis. The other organs can only grow if gross photosynthesis exceeds the sum of maintenance respiration and leaf growing sink.
(2) from leaf maturity to complete yellowing (end of senescence): If net photosynthesis (i.e. gross photosynthesis minus autotrophic respiration) is positive, the allocation to all parts of the tree is allowed according to constant coefficients for each organ. Otherwise, no growth is allowed and storage is used for maintenance respiration.
(3) from the end of leaf senescence to budburst: source is the storage compartment, sink is the maintenance respiration and no growth occurs.

Vegetative growth of forests may be temperature limited in temperate environment (Cannell et al., 1988). However, except for leaves (see above), no direct effect of temperature on growth has been incorporated in the model. The water stress effect operates only indirectly by reducing gross photosynthesis. Moreover, there are no age-related effects on carbon allocation besides the indirect effect of increasing living biomass.

The partitioning model is somehow simplistic, since we assume constant partionning coefficients for aerial wood, fine roots, coarse roots and reserves (following McMurtrie and Wolf, 1983). It corresponds to the empirical approach described in Thornley and Johnson (1990). But it requires very few parameters compared with more mechanistic approaches as the transport-resistance mechanistic models. Moreover, it seems quite efficient, for a given site and one year (see Part II). However, if one want to take into account the age (Magnani et al., 2000) and fertility (McMurtrie, 1985) effects on the allocation processes, the allocation coefficients may be calculated by adding empirical or functional constraints on the sinks (e.g. fine roots to leaf ratios) as in Barbaroux (2002) and Davi (2004).

2.6.1. Sunlit leaf mass per area (LMA) evolution

The evolution of sunlit leaf mass per area (LMA_{Sun}) is simulated in the same way as the leaf area index (L), with a dependency on air temperature. A higher critical value of state of forcing $F_{crit\ LA}$ is used to calculate the end of LMA growth.

$$S_{frcLMA} = \sum_{N_{BB}}^{N_{LMAmax}} T \qquad \text{if} \qquad T > T_3 \tag{20}$$

$$LMA_{Sun} = \frac{S_{frcLMA}}{F_{critLMA}} \times LMA_{Sunmax} \tag{21}$$

S_{frcLMA} is the state of forcing for leaf mass growth, LMA_{Sunmax} the maximum value of sunlit leaf mass per area reached during the year and N_{LMAmax} the day when LMA_{Sun} reaches LMA_{Sunmax}. Note that LMA_{Sunmax} is an input parameter and then it varies according to the site and the species.

The foliar biomass is then calculated as the integral over the canopy of leaf mass per area times the leaf area index.

$$B_{leaf} = \int_0^{L_{max}} LMA_L \, dL \tag{22}$$

Then the foliar growth (GB_{leaf}) (which, if negative, turns out to be the mortality MB_{leaf}), is calculated as the difference between foliar biomass (B_{leaf}) of the day and foliar biomass of the previous day.

2.6.2. Carbon allocation to the different compartments

After accounting for leaf growth and need of carbohydrate for maintenance respiration, the available carbon is allocated to the four other compartments (aerial woody organs, storage, coarse roots and fine roots). The carbon growth of the different organs but leaves (GB_{organ}), is a proportion (allocation coefficients) of the available carbon during the same day:

$$GB_{organ} = \frac{AG_{organ}}{CR_{organ}} \times (A_{canopy} - RM - RG_{leaf} - GB_{leaf}) \tag{23}$$

AG_{organ} is the allocation coefficient per organ type (the sum of the four coefficients is one), A_{canopy} the gross canopy photosynthesis, CR_{organ} the organs construction cost (see growth respiration), RM the total maintenance respiration (all organs), RG_{leaf} the leaf growth respiration and GB_{leaf} the leaf growth.

During the leafy period, if maintenance respiration (RM) is greater than gross photosynthesis, the required carbon is taken from storage ($MB_{storage}$, "storage emptying"). During the leafless period, all the carbon needed for maintenance respiration contribute to storage emptying.

$$\frac{dB_{storage}}{dt} = GB_{storage} - MB_{storage} \tag{24}$$

The fine roots mortality depends on a constant turn over ($TO_{fine\ roots}$) and on the fine roots biomass ($B_{fine\ roots}$). The fine roots biomass is thus given by:

$$\frac{dB_{fine\ roots}}{dt} = GB_{fine\ roots} - TO_{fine\ roots} \times B_{fine\ roots} \tag{25}$$

The mortality of woody organs (branches, trunk and coarse roots) is not simulated. Hearthwood formation (i.e. duramenisation) is not taken in consideration seasonally but only annually. The equations of daily biomass evolution are therefore:

$$\frac{dB_{organ}}{dt} = GB_{organ} \tag{26}$$

The distribution of aerial woody biomass between stems and branches depends on an allometric coeffi-

cient P_{branch} which is function of stand age and species.

$$B_{branch} = P_{branch} \times B_{aerial\ wood} \quad (27)$$

The living biomass of woody organs ($B_{alive\ organ}$, i.e. trunk, branches and coarse roots) is calculated each day after growth calculation using the proportion of living wood ($P_{alive\ organ}$). This living biomass is used to estimate maintenance respiration and changes with species and age.

$$B_{alive\ organ} = P_{alive\ organ} \times B_{organ} \quad (28)$$

2.7. Maintenance respiration

Maintenance respiration is calculated from the nitrogen content of living biomass and assuming an exponential relationship to account for temperature dependence (Ryan, 1991). For each compartment (i.e. type of organ) maintenance respiration is simulated every half hour.

$$RM_{organ} = B_{alive\ organ} \times MRN \times N_{morgan} \times Q_{10\ organ}^{(Tsuf - T_{MR}/10)} \quad (29)$$

where T_{surf} is the surface temperature, $B_{alive\ organ}$ the biomass of living tissue actually respiring, N_{morgan} the amount of nitrogen per alive mass unit and MRN the respiration rate per nitrogen unit. Q_{10} of aerial woody parts (i.e. trunk and branch) is different from other compartments.

During the night, the foliar respiration is calculated using Eq. (29). During the day, light is assumed to inhibit this respiration according to a constant ratio $P_{leaf\ inhib}$. The degree of inhibition ranges between 17 and 66% depending on species (Sharp et al., 1984; Brooks and Farquhar, 1985; Kirschbaum and Farquhar, 1987). Villar et al. (1995) give a mean rate of 51% for evergreen tree species and 62% for deciduous tree species.

2.8. Growth respiration

Organ growth is calculated on a daily time step and, consequently, growth respiration is first calculated on a daily basis ($RG_{d\ organ}$), assuming that daily growth respiration depends on both growth rate (GB_{organ}) and construction cost (CR_{organ}) of the considered organ. The construction cost can be calculated from gas exchange measurements or following the approach of Penning de Vries et al. (1974) and Penning de Vries (1975a, 1975b), based on the knowledge of the organ biochemical composition (i.e. nitrogen, lignin, lipids, organic acids, carbohydrates, total mineral content).

$$RG_{d\ organ} = GB_{organ}(CR_{organ} - 1) \quad (30)$$

During a second step, growth respiration is calculated half-hourly assuming that surface temperature is the driving variable (Q_{10}-based relationship). We can then calculate the net ecosystem CO_2 flux (NEE) on an half-hourly time step.

2.9. Water fluxes

2.9.1. Rainfall interception by the canopy

The canopy is regarded as having a surface storage capacity, recharged by rainfall and discharged by evaporation and drainage. The storage capacity of leaves and woody parts (i.e. stems and branches) are considered separately. During the leafy period, leaves intercept a fraction of rainfall, depending on both leaf area index and gap fraction. If the amount of water intercepted exceeds the leaf capacity storage, the excess is lost by throughfall and can either be intercepted by woody parts or reach the soil surface. If the amount of rainfall intercepted by woody parts exceeds the storage capacity of the bark then water can both run out along branches and stems or throughfall on to the litter layer. Evaporation rate occurs according to the Penman–Montheith equation (Monteith, 1965) assuming a zero stomatal resistance.

$$R_{leaf\ max} = L \times RA_{leaf} \quad (31)$$

$$R_{bark\ max} = 2 \times WAI \times RA_{bark} \quad (32)$$

$$R_{can\ max} = R_{bark\ max} + R_{leaf\ max} \quad (33)$$

$R_{leaf\ max}$, $R_{bark\ max}$, and $R_{can\ max}$ are respectively the bark, leaf and canopy water storage capacity. L and WAI are respectively leaf and wood area indices. RA_{leaf} and RA_{bark} are respectively the water storage capacity per unit of leaf and bark area.

The gross water interception of leaves (I_{leaf}) and barks (I_{bark}) depends on precipitation (Pi) and interception coefficients for leaves (C_{leaf}) and bark (C_{bark})

respectively:

$$I_{leaf} = C_{leaf} \times Pi \quad (34)$$

$$I_{bark} = C_{bark} \times Eg_{leaf} \quad (35)$$

during leafy period (if $L > WAI$). Eg_{leaf} is the drainage occurring, when the water on the leaf exceeds the leaf storage capacity.

$$I_{bark} = C_{bark} \times Pi \quad (36)$$

during leafless period (if $L < WAI$)

$$C_{leaf} = \frac{L}{L \times C_{ia} + C_{ib}} \quad (37)$$

$$C_{bark} = \frac{WAI}{WAI \times C_{ia} + C_{ib}} \quad (38)$$

C_{ia} and C_{ib} are empirical coefficients.

R_{leaf}, R_{bark} and R_{can} are respectively the current bark, leaf and canopy (bark + leaves) water reserve, which are calculated half hourly by summing gross water interception (respectively I_{leaf} and barks I_{bark}).

If the amount of water on bark (R_{bark}) exceeds the storage capacity ($R_{bark\,max}$) then drainage occurs and the excess of water is separated into two parts: the first one flowing along the bark (Ec) and the other one dripping over the soil (Eg_{bark}). Allocation between flows is determined with an empirical coefficient ($PROP_{EC}$).

Then the net rainfall interception of the canopy (IN), the rain falling directly on the soil through the canopy (PSd_{soil}) and the total amount of precipitation reaching the soil (PS_{soil}) are calculated:

$$IN = (I_{leaf} - Eg_{leaf}) + (I_{bark} - Eg_{bark} - Ec) \quad (39)$$

$$PS_{soil} = Pi - IN \quad (40)$$

$$PSd_{soil} = PS_{soil} - Eg_{leaf} \times (1 - C_{bark}) - Eg_{bark} - Ec \quad (41)$$

2.9.2. Canopy evapotranspiration

Following Rutter et al. (1971) and Chassagneux and Choisnel (1986, 1987), the canopy evapotranspiration (ETR_{canopy}) is calculated by adding water evaporated (EP) from the wet parts of the canopy and transpiration (Tr) from the dry parts:

$$ETR_{canopy} = \left(\frac{R_{can}}{R_{canmax}}\right) \times EP + \left(1 - \frac{R_{can}}{R_{canmax}}\right) \times Tr \quad (42)$$

R_{can} represents the current quantity of water retained by the canopy (i.e. bark + leaves) and R_{canmax} the storage capacity. The Penman–Monteith equation (Monteith, 1965) is applied at the canopy level to calculate both transpiration (Tr) and evaporation (EP).

$$Tr = \frac{\Delta h \times Rn_{veg} + (\rho_{cp} \times C_{ph} \times VPD)/R_{ac}}{\lambda h(\Delta h + \gamma \times (1 + 1/(g_c \times R_{ac})))} \quad (43)$$

Heat storage and soil heat flux are assumed to be negligible. The canopy conductance g_c is calculated by averaging leaf stomatal conductance over the canopy. For water evaporation calculation, an infinite conductance g_c is assumed (no resistance) and Eq. (43) is simplified to the Penman formulation (Penman, 1948) modified by Van Bavel (1966). Net radiation (Rn_{veg}) is driven by energy balance (see radiative balance in the global domain), air vapour pressure deficit (VPD) is an input meteorological variable and the canopy aerodynamic resistance (R_{ac}) is calculated assuming a logarithmic wind profile above the canopy and an exponential decrease inside the canopy (adapted from Lafleur and Rouse, 1989). λh is latent heat; Δh is the slope of the relation between saturate vapor pressure and surface temperature, γ is the psychometric constant; ρ_{cp} is the air density and C_{ph} the air specific heat. All of these parameters vary according to the temperature except C_{ph}.

2.9.3. Soil evaporation

Soil evaporation (EP_{soil}) is calculated in the same way as canopy transpiration using Penman–Monteith equation. It differs from canopy evaporation only by the available energy for evaporation (Rn_{soil}), the aerodynamic resistance from soil to atmosphere (R_{as}) and the water vapour soil conductance (g_{soil})

Soil conductance to water vapour depends on water status both in the upper part of soil (RW_{top}) and in litter (RW_{lit}).

$$g_{soil} = (g_{soil\,max} - g_{soil\,min}) \times \frac{RW_{top} - RW_{top\,wilt}}{RW_{top\,fc} - RW_{top\,wilt}} + g_{soil\,min} \quad (44)$$

$g_{soil\,max}$ is the maximal soil conductance which is a site specific constant. Note that when leaf litter above top soil is wet, g_{soil} is taken to $g_{soil\,max}$ value. $RW_{top\,fc}$ is the water content at field capacity of upper part of soil. $RW_{top\,wilt}$, the water content at wilting point upper

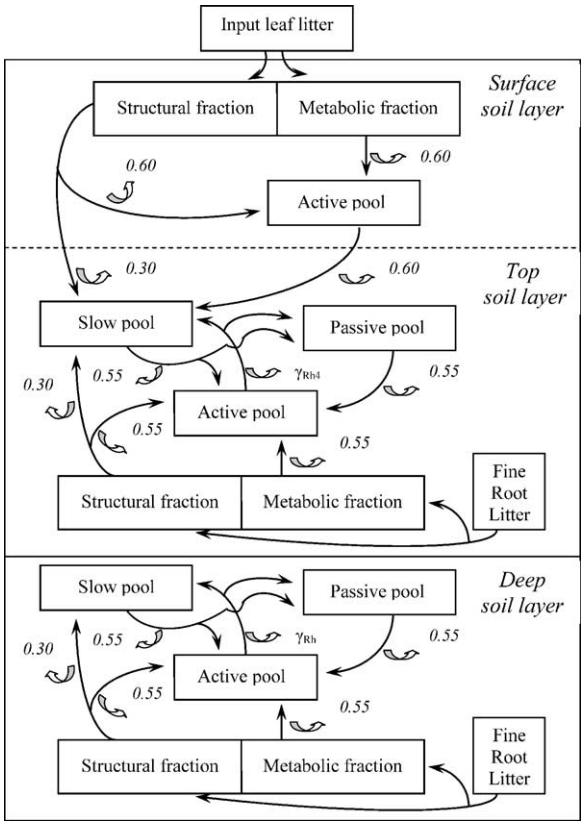

Fig. 2. Flow diagram for the soil carbon sub-model. Each boxes is a state variable for soil carbon (i.e. soil organic matter compartments). Except input from leaf and root litters, each arrow (simple) correspond to a carbon flow (decomposition rate) from one compartment to the next one with the double arrow output corresponding to the proportion of flow respired (heterotrophic respiration). γ_{Rh4} depends on soil textural properties.

part of soil. When litter and top-soil layers are dry, evaporation is limited according to $g_{\text{soil min}}$.

2.9.4. Soil water balance

The soil water balance model (see Fig. 2) is basically a bucket one with three layers (litter, a top-soil layer and a total-soil root zone including top-soil layer). Current water contents (RW_{lit}, RW_{top}, RW_{soil}) are the state variables corresponding to the three compartments. For each layer, water content is calculated daily as the difference between inputs (stemflow, throughfall and drainage from above layer) and outputs (evaporation, transpiration and drainage). The way to arrange in time the different fluxes is different for litter and soil compartments:

- Litter*:* three steps are considered

– Input: incoming water is the sum of throughfall and rain reaching directly the soil through the canopy. Note that the water flowing along the bark (Ec) goes directly to the top-soil.

$$\begin{aligned}\text{RW}_{\text{lit int}} &= \text{RW}_{\text{lit}(t-1)} + \text{PSd}_{\text{soil}} + \text{Eg}_{\text{leaf}} \\ &\quad \times (1 - C_{\text{bark}}) + \text{Eg}_{\text{bark}} \end{aligned} \tag{45}$$

$RW_{lit\,int}$ is an intermediate variable (transitory water content before evaporation and drainage).

– Output 1: evaporation of litter (E_{lit}).

$$E_{\text{lit}} = \min(\text{EP}_{\text{soil}}; \text{RW}_{\text{lit int}}) \tag{46}$$

– Output 2: after evaporation and interception, if RW_{lit} exceeds the water litter content at "field capacity" ($RW_{lit\,fc}$) then water drains down (D_{lit}) to the top-soil layer:

$$D_{\text{lit}} = \max(\text{RW}_{\text{lit int}} - E_{\text{lit}} - \text{RW}_{\text{lit fc}}; 0) \tag{47}$$

$$\begin{aligned}\text{RW}_{\text{lit}(t)} &= \text{RW}_{\text{lit}(t-1)} + \text{PSd}_{\text{soil}} + \text{Eg}_{\text{leaf}} \\ &\quad \times (1 - C_{\text{bark}}) + \text{Eg}_{\text{bark}} - D_{\text{lit}} - E_{\text{lit}} \end{aligned} \tag{48}$$

- *Soil:* 2 steps are considered
Note that two water balances are calculated independently; one for the top-soil layer and another one for the total soil root zone (including top soil layer). Both are used to calculate the soil water stress (see below Eq. (56)), which controls both transpiration and photosynthesis.

– Input: stemflow (Ec) and litter drainage (D_{lit}).
For each layer (j), a temporary water content is calculated:

$$\text{RW}_{\text{int}}(j) = \text{RW}_{(d-1)}(j) + \text{Ec} + D_{\text{lit}} \tag{49}$$

For each soil layer, the water content at day d $RW_{(d)}$ is calculated as the product of actual soil volumetric humidity (θ) and the layer thickness H(l).

$$\text{RW}_{\text{fc}}(j) = \theta_{\text{fc}}(j) \times H(j) \tag{50}$$

$RW_{fc}(j)$ is the water content at field capacity of the layer (j). $RW_{wilt}(j)$, the water content at wilting point, is calculated in the same way.

– Output: soil water drainage ($D(j)$), soil evaporation ($E(j)$) and canopy transpiration TR(j), for the layer (j):

$$D(j) = \max(\mathrm{RW}_{\mathrm{int}}(j) - \mathrm{Ec} - \mathrm{RW}_{\mathrm{fc}}(j); 0) \quad (51)$$

$$\mathrm{RW}_{(d)}(j) = \mathrm{RW}_{(d-l)}(j) + \mathrm{Ec} + D_{\mathrm{lit}} - D(j) - E(j) - \mathrm{TR}(j) \quad (52)$$

$$E(j) = \mathrm{EP}_{\mathrm{soil}} - E_{\mathrm{lit}} \quad (53)$$

$$\mathrm{TR}_{\mathrm{top}} = \mathrm{prac} \times \mathrm{TR} \quad (54)$$

where prac is the proportion of fine roots in top soil layer, depending on soil type and soil depth.

2.10. Effect of soil water status on canopy gas exchange

During water stress period the slope (g_1) of the relationship, proposed by Ball et al. (1987) between leaf assimilation (A) and stomatal conductance (gs) (Eq. (4)), is assumed to decrease linearly when soil water storage decreases (Sala and Tenhunen, 1996). The effect of soil water stress on photosynthesis translates into g_1 through a reduction factor (reduc):

$$g_1 = (g_{1\max} - g_{1\min}) \times \mathrm{reduc} + g_{1\min} \quad (55)$$

$g_{1\min}$ and $g_{1\max}$ are respectively the minimum and maximum values taken by g_1. While the water content of one of the soil layer (j) is above a specific threshold based on proportion of soil extractable water content ($S_{\mathrm{stress}} \times [\mathrm{RW}_{\mathrm{fc}}(j) - \mathrm{RW}_{\mathrm{wilt}}(j)] + \mathrm{RW}_{\mathrm{wilt}}(j)$) then no water stress occurs (i.e. reduc = 1). On the contrary when both soil layers (top and total) are below this threshold, the soil water stress increase linearly with decreasing soil water content until zero:

$$\mathrm{reduc} = \left(\frac{\mathrm{RW}_{\mathrm{soil}} - \mathrm{RW}_{\mathrm{soil\,wilt}}}{S_{\mathrm{Stress}}(\mathrm{RW}_{\mathrm{soil\,fc}} - \mathrm{RW}_{\mathrm{soil\,wilt}})} \right) \quad (56)$$

RW(j), $\mathrm{RW}_{\mathrm{wilt}}(j)$ and $\mathrm{RW}_{\mathrm{fc}}(j)$ are respectively the water content, the water content at wilting point and the water content at field capacity for the considered soil layer (j). S_{Stress} is a threshold parameter for soil water stress.

2.11. Heterotrophic respiration and soil organic matter

The soil organic carbon sub-model (SOC), based on the soil organic matter (SOM) sub-model of CENTURY (Parton et al., 1987), simulates the dynamic of carbon in the soil system at the daily time step. Soil organic carbon is divided into three major components including active, slow and passive soil carbon. Active SOC includes live soil microbes plus microbial products, the slow pool includes resistant plant material (lignin-derived material), soil-stabilized plant and microbial material. The passive material is very resistant to decomposition and includes physically and chemically stabilized SOM. The model also includes a surface microbial pool, which is associated with decomposing surface litter (mainly leaf litter). Carbon flows between these pools are controlled by decomposition rate and microbial respiration loss parameters, both of which are a function of soil texture, soil temperature and soil water content.

The original version developed by Parton et al. (1987) has been adapted to be coupled with the forest plant sub-model (Le Dantec, 2000; Epron et al., 2001). In this soil model, all fractions are located in the soil vertical profile (see Fig. 2). The soil is divided into three layers according to the soil water balance sub-model. A deep soil layer, however, is considered explicitly rather than a total soil layer (see Fig. 1). The first layer is the surface litter one, containing both metabolic and structural fractions (calculated from leaf litter input) and the associated microbial pool. The top (0–30 cm) and the deepest layer (below 30 cm) include all carbon pools, i.e. the microbial population (active pool), both metabolic and structural fractions of root litter, and the slow and passive soil organic carbon.

The carbon inputs from plant residue (leaves and fine roots) are simulated by the plant phenology sub-model. Surface layer receives the leaf litter and soil layers receive the root litter in proportion of root biomass (i.e. assuming a similar mortality rate for each layer). No carbon migration is assumed between the superficial and the deep soil layers. The “slow pool” of the superficial layer, however, is supplied with the organic carbon coming from both the structural fraction and the active SOC of the surface layer.

For the different pools (i), the decomposition rate (DR) is the output flow:

$$DR_{(i)}(j) = K_{(i)}(j) \times Q_{(i)}(j) \times A_w(j) \times A_t(j) \times C_{(i)}(j) \quad (57)$$

where j is the soil layer where the considered carbon pool i is located.

According to Parton et al. (1987), K is the maximum decomposition rate, C the carbon biomass, A_w and A_t, the impact function of soil water content and temperature respectively. Q depends on soil textural properties of the considered j layer for the soil active and slow carbon pools; it depends on lignin content of the considered litter (leaves or fine roots) for the litter structural material, and it equals 1 for the other carbon pools.

$$A_w(j) = \frac{1}{(1 + 30e^{-8.5 \times RW(j)/[RW_{fc}(j) - RW_{wilt}(j)]})} \quad (58)$$

where RW(j) is the soil water content of the layer (j), simulated by the soil water balance model. $RW_{wilt(j)}$ and $RW_{fc(j)}$ are the soil water content at wilting point and at field capacity respectively for the considered layer.

$$A_T(j) = \left[\frac{45 - T(j)}{45 - T_b(j)}\right]^{0.2} \times e^{0.076(1-[(45-T(j))/(45-T_b(j))]^{h(j)})} \quad (59)$$

where $T(j)$ is the temperature of the considered layer, T_b (j) a base temperature depending on soil layer and $h(j)$ a parameter depending on soil layer.

The model assumes that all C decompositions flows (DR) are associated with microbial activity and that microbial respiration occurs for each of these flows. Heterotrophic soil respiration ($R_{heterotrophic}$) is the sum of all these microbial respiration processes. Depending on the considered soil C pool (see Fig. 2), output flows can be separated into two parts according to lignin content (flows from structural fraction of litter) or with textural composition of the soil layer (flows from both active and slow soil pools).

2.12. Calculation of CO_2 fluxes: NPP (Net Primary Productivity) and NEE (Net Ecosystem Exchange)

$$NPP = A_{canopy} - RM - RG \quad (60)$$

$$NEE = NPP - R_{heterotrophic} \quad (61)$$

A_{canopy} is the canopy gross phototosynthesis, RM the maintenance respiration of all organs, RG the growth respiration of all organs and $R_{heterotrophic}$ the soil heterotrophic respiration.

3. In situ measurements (Hesse, France, 1997)

3.1. Site characteristics

The experimental plot area is located in the State forest of Hesse (East of France; 48°40′N, 7°05′E), and is mainly composed of beech (*Fagus sylvatica* L.); understorey vegetation is very sparse. The elevation is 300 m and the slope is less than 2%. The studied plot covers 0.63 ha of a pole beech forest (30 years old in 1997) with a density of 3482 trees ha^{-1} and a dominant height close to 14 m. Three towers were installed: one (18 m high) is used for eddy covariance and microclimate measurements, the two other ones (15 m high) for physiological measurements. A hut containing the data acquisition systems is located near the first tower. Sixty sub-plots are delimited for geo-statistical studies of soil and vegetation. For more details, see Granier et al. (2000a).

3.2. Model parameterization data set

3.2.1. Meteorological driving variables

Micro-meteorological sensors are installed above the stand at a height of 17.5 m: a global radiometer (Mod 180, Cimel, France), a laboratory-made quantum sensor (Pontailler and Genty, 1996), a ventilated psychrometer (INRA, with Pt 100), a raingauge (ARG 100, Campbell Scientific, Logan, Utah), and a switching anemometer (Vector Instruments, UK). Additionally, soil temperature sensors (copper/constantan thermocouples) are installed at −10 cm (five replicates) and in one profile (−5, −10, −20, −40, and −80 cm) in a central plot. Weather data were averaged/summed and recorded half-hourly using an acquisition system (Campbell Scientific) (see Table 3).

3.2.2. Species and site-specific parameters

Values of the main input parameters are given in Table 1 and initial values of state variables are given in Table 2.

Table 2
List of state variables

Symbol	Description	Units	Initial value	Reference
Carbon plant				
B_{leaf}	Leaf biomass	$g_C\ m_{soil}^{-2}$	0	
B_{branch}	Branch biomass	$g_C\ m_{soil}^{-2}$	519	Damesin et al. (2002)
B_{trunk}	Trunk biomass	$g_C\ m_{soil}^{-2}$	3691	Damesin et al. (2002)
$B_{coarseroot}$	Coarse roots biomass	$g_C\ m_{soil}^{-2}$	815	Le Goff and Ottorini (2001)
$B_{fineroot}$	Fine roots biomass	$g_C\ m_{soil}^{-2}$	171	Bauhus and Bartsch (1996)
$B_{storage}$	Carbohydrate storage biomass	$g_C\ m_{soil}^{-2}$	160	Barbaroux (2002)
Carbon soil (three layers: surface litter, top and deep soil)				
C_m (lit)	Metabolic fraction of litter (leaves)	$g_C\ m_{soil}^{-2}$	43	Epron et al. (2001)
C_{St} (lit)	Structural fraction of litter (leaves)	$g_C\ m_{soil}^{-2}$	335	Epron et al. (2001)
C_a (lit)	Active C pools (micro-organism) of litter	$g_C\ m_{soil}^{-2}$	35	Epron et al. (2001)
C_m (top)	Metabolic fraction of top soil (fine roots litter)	$g_C\ m_{soil}^{-2}$	22	Epron et al. (2001)
C_{St} (top)	Structural fraction of top soil (fine roots litter)	$g_C\ m_{soil}^{-2}$	320	Epron et al. (2001)
C_a (top)	Active C pools (micro-organism) of top soil	$g_C\ m_{soil}^{-2}$	230	Epron et al. (2001)
C_S (top)	Slow C pools of top soil	$g_C\ m_{soil}^{-2}$	2833	Epron et al. (2001)
C_P (top)	Passive C pools of top soil	$g_C\ m_{soil}^{-2}$	827	Epron et al. (2001)
C_m (deep)	Metabolic fraction of deep soil (fine roots litter)	$g_C\ m_{soil}^{-2}$	7	Epron et al. (2001)
C_{St} (deep)	Structural fraction of deep soil (fine roots litter)	$g_C\ m_{soil}^{-2}$	113	Epron et al. (2001)
C_a (deep)	Active C pools (micro-organism) of deep soil	$g_C\ m_{soil}^{-2}$	104	Epron et al. (2001)
C_S (deep)	Slow C pools of deep soil	$g_C\ m_{soil}^{-2}$	1442	Epron et al. (2001)
C_P (deep)	Passive C pools of deep soil	$g_C\ m_{soil}^{-2}$	2400	Epron et al. (2001)
Water				
R_{leaf}	Amount of water on leaves in the canopy	mm	0	
R_{bark}	Amount of water on bark	mm	0	
RW_{lit}	Amount of water in soil surface litter	mm	0	
RW_{top}	Amount of water in top soil layer	mm	$RW_{top\ fc}$	
RW_{soil}	Amount of water in the deep soil layer	mm	$RW_{soil\ fc}$	

3.2.3. Stand and canopy structure

Initial biomass of organs have been determined by inventories of aerial (see Granier et al., 2000a) and below-ground tree parts (Le Goff and Ottorini, 2001) or by an estimation from literature for fine roots less than 2 mm diameter (Bauhus and Bartsch, 1996). The amount of carbohydrate stored was estimated from measurement on the different woody organs (Barbaroux et al., 2003).

Maximum leaf area index (L_{max}) was estimated by litter collection during leaf fall (42 square litter traps, 0.25 m^2 each) (Granier et al., 2000a). Foliage aggregation was calculated by dividing an apparent leaf area index measured using a plant canopy analyzer (LAI2000, Li-Cor, Lincoln, Nebraska), calculated with four rings, by the true leaf area index derived from litter collection. Wood area index was calculated using allometric relationships between both trunk and branch area with trunk girth measured at 1.30 m height (Damesin et al., 2002).

A profile of leaf mass per area was measured at end of June in 1997 (Montpied, personaal communication) allowing us to calculate the coefficient k_{LMA}, which is close to those observed in other canopies (Aussenac

Table 3
List of external forcing variables

Symbol	Description	Units
Meteorological variables changing half-hourly		
PAR	Photosynthetic active radiation (400–700 nm)	μmol photons $m^{-2}\ s^{-1}$
R_g	Global shortwave radiation (400–2500 nm)	$W\ m^{-2}$
RH	Air relative humidity	Dimensionless
T_a	Air temperature	°C
V	Wind speed	$m\ s^{-1}$
P_i	Incident rainfall	mm
T_{soil} (top)	Top soil temperature	°C
T_{soil} (deep)	Deep soil temperature	°C

and Ducrey, 1977; Ducrey, 1981; Rambal et al., 1996).

3.2.4. Rainfall interception and canopy evaporation rate

Bark water storage capacity ($R_{barkmax}$) was estimated from literature data on smooth bark species, by dividing canopy water storage (0.3–0.65 mm) during leafless period (Helvey and Patric, 1965; Leyton et al., 1967) by wood area derived from allometric relationship (Damesin et al., 2002). We used leaf water storage capacity ($R_{leafmax}$) given by Nizinski and Saugier (1988) for *Quercus petraea*. We obtain water storage during leafless ($R_{barkmax}$) period of 0.45 mm and canopy water storage during leafy period of 1.6 mm (very similar to the threshold value of 1.7 mm given by Granier et al., 2000b).

Interception coefficients for leaves (C_{leaf}) and woody parts (C_{bark}) were estimated using gap canopy fractions measured over 0–20° zenithal angle from hemispherical photography. Then parameters C_{ia} and C_{ib} were calculated by solving Eqs. (37) and (38).

Allocation between stemflow and drainage ($PROP_{EC}$) was calibrated using data measured during the leafy period of 1997 (Granier et al., 2000b).

3.2.5. Maintenance respiration

Temperature dependency (Q_{10}) for bole and branches was measured in Hesse forest by Damesin et al. (2002). We used the same value of Q_{10} for coarse roots as for bole wood. For other organs, fines roots and leaves, we used Q_{10} values from literature, respectively from Epron and Badot (1997) and from Vose and Bolstad (1999).

Bole and branches nitrogen concentrations (N_m) were measured in situ (Ceschia et al., 2002). Profiles of N_m in leaves were measured by P. Montpied (personal communication) showing little variation with leaf layer. N_m in coarse roots was taken the same as for bole wood. For fine roots we used nitrogen concentration from Van Praag et al. (1988).

We used the nitrogen dependency given by Ryan (1991) to calculate the basal respiration (i.e. respiration at base temperature, here 15 °C).

3.2.6. Phenology

To derive phenological parameters, we used observations and measurements performed on beech plots in Fontainebleau forest (France). For budburst we used a 17-year data set, for leaf growth and leaf fall we used 4 years LAI values, measured at regular intervals along the leafy periods (Li-Cor LAI 2000) and 9 years of semi-quantitative leaf yellowing observations. Despite that budburst models generally do not work very well for beech species (Kramer, 1994), the accuracy of the obtained prediction is better than the null hypothesis which is not the case of different models tested by Kramer (1994). This is specific to *Fagus sylvatica* because our model performs very well for both sessile oak and hornbeam phenology measured using the same protocol in the Fontainebleau forest (data not shown). The data set used to parameterise leaf growth and leaf fall is small. However, as the leaf growth is very fast (less than 3 weeks for beeches), the influence of the function and the parameters used is not crucial. Leaf yellowing is more variable from year to year according to late seasonal water stress influence. Consequently the parameterisation could possibly be improved by adding more observations.

Few data are available for LMA dynamic during leaf maturation phase on mature beech trees: measurements in the Italian site of Collelongo in 1995 (Matteucci, 1998), a study from Schulte (1993) in the German site of Solling (1986–1988), an unpublished experiment on mature trees during spring 1998 in Orsay (France) and a monitoring in Hesse in 1998 (Montpied, personal communication). We determined the critical value of state of forcing (from budburst to leaf maturity) by averaging results from all experiments (424 °C/day ± 81).

3.2.7. Allocation of assimilates

Leaf allocation is predicted by the phenology submodel. We used the coefficient for storage allocation estimated by Barbaroux (2002). The coefficient for fine roots was estimated by inversing the model and assuming a constant biomass on a yearly basis. Finally the coefficient for coarse roots was deduced assuming a constant ratio of 0.2 between coarse roots and trunks.

3.2.8. Mortality of organs

Leaf mortality is simulated by the phenology submodel. Fine roots mortality is assumed to be proportional to the biomass with a turnover of 1 over the year (Bauhus and Bartsch, 1996). We assumed no bole or branches mortality over one year simulation.

3.2.9. Growth respiration

For aerial woody organs, the construction cost is calculated using both respiration and growth measurements (Damesin et al., 2002). The construction cost for coarse roots is considered to be the same as for bole. For leaves and fine roots, data from literature were used (Niinemets, 1999; Ågren and Axelsson, 1980 respectively).

3.2.10. Soil water balance

During 1997, the soil volumetric water content (θ) was measured weekly with a neutron probe (NEA, Ballerup, Denmark) along eight aluminium access tubes of 160 cm long. The volumetric minimum water content (θ_{wilt}) and the water content at field capacity (θ_{fc}) were estimated for both top and deep soil layers. For each soil layer, θ_{fc} was taken as the average observed θ during the winter when soil was refilled (after a delay of one day to take into account of rapid drainage) and θ_{wilt} was estimated from retention curves.

The height of total soil root zone (H_{soil}) is assumed to be 160 cm in Hesse (Granier et al., 2000b). The height of the upper soil layer (H_{top}) is set to 30 cm, corresponding to the part of the soil which is more dynamic in terms of volumetric water content evolution and contributes more to the stomata control (Dufrêne, 1989). The upper soil layer includes 63% of fine roots (Quentin et al., 2001). This value is similar to those given for temperate deciduous species by Jackson et al. (1997).

Very few data regarding soil water vapour conductance of forest are available in the literature. No measurements were done on Hesse forest and consequently the minimum soil vapor conductance (g_{solmin}) was taken equal to the value given by Schaap et al. (1997) and the maximal soil vapour conductance (g_{solmax}) was derived from Kelliher et al. (1986). These two values were measured in a Douglas fir stand.

The soil water stress threshold (S_{Stress}) is not very variable according to soil and species (see review from Granier et al., 1999) and the value was fixed to 0.4.

3.2.11. Soil heterotrophic respiration and organic matter

The soil mineral composition and the soil total carbon content were measured in situ (Farque, 1997). The initialization of the different carbon pools was set from the vertical distributions of carbon concentrations and of residence times in soil (Elzein and Balesdent, 1995), and from the vertical distribution of microbial biomass in soil (Wolters and Joergensen, 1991; Ross et al., 1996). Equilibrium values for carbon pools obtained after 20-year simulation periods were used to initialize the sub-model (Epron et al., 2001).

3.3. The eddy covariance data set

From January through December 1997, CO_2 fluxes were measured in a meteorological tower at 18 m (i.e 3 m above the canopy) using the eddy covariance method (Leuning and Moncrieff, 1990). A complete description of the system used is given by Granier et al. (2000a).

4. Sensitivity analysis methodology

CASTANEA uses many input parameters; some are coming from literature, other ones are specifically fixed. Most of these parameters are estimated from field sampling, fitting curve technique, interpolation or theoretical evaluation. It is important to identify the input parameters having the greatest effect on model predictions, and to quantify the uncertainty in the model predictions due to the combined effects of uncertainties in the set of input parameters. In this study, the Net Ecosystem Exchange, which sums up most of the model processes, was chosen as the main output variable. The sensitivity study and the subsequent uncertainty study are based on the Monte Carlo technique. The principle was described in Spear and Hornberger (1980) and further developed in Franks and Beven (1997), and applied in Franks et al. (1999). In our study, each parameter is associated with a randomly set error and an ensemble of simulation is performed by a random selection of input parameter values following a Gaussian distribution. Haan et al. (1998) have evaluated the impact of parameter distribution assumptions on estimates of model output uncertainty and concluded that good estimates of the means and variances of the input parameters are of greater importance than the actual form of the distribution (Haan et al., 1998).

Three successive steps are carried out: (i) identification of key parameters through a sensitivity analysis involving all parameters, (ii) determination of the real uncertainty on the key input parameters, and (iii) uncer-

tainty analysis involving all the selected key parameters together.

The results of such a study could depend on the site, soil and climate that are considered. Our sensitivity and uncertainty analysis applies to the Hesse site for the year 1997, using the above described parameterisation.

4.1. Determination of the key input parameters

In the first step, our purpose was to identify key input parameters, i.e. the parameters whose variations have the largest effect on the model outputs. For this purpose, we applied a +10% or −10% bias on each of the 146 parameters and 23 initial conditions of state variables (Table 2).

For each parameter and initial state variables, we calculated the difference between the Net Ecosystem Exchange computed with +10% (respectively −10%) of a chosen parameter and the reference $\mathrm{run}_{\mathrm{no\ bias}}$. Subsequently the percent of variation ($\mathrm{VR}_{+10\%}$ and $\mathrm{VR}_{-10\%}$) were calculated as:

$$\mathrm{VR}_{+10\%} = 100 \times \frac{|\mathrm{run}_{\mathrm{no\,bias}} - \mathrm{run}_{+10\%}|}{\mathrm{run}_{\mathrm{no\,bias}}} \quad (62)$$

$$\mathrm{VR}_{-10\%} = 100 \times \frac{|\mathrm{run}_{\mathrm{no\,bias}} - \mathrm{run}_{-10\%}|}{\mathrm{run}_{\mathrm{no\,bias}}} \quad (63)$$

The maximum percent of variation between $\mathrm{VR}_{+10\%}$ and $\mathrm{VR}_{-10\%}$ was used to represent the effect of the parameter (or of the initial condition) on the annual NEE.

Afterwards, the parameters and initial conditions were sorted in descending order according to the effect on NEE. All initial conditions and parameters with an effect of more than 2.5% on NEE were kept for the uncertainty analysis.

4.2. Estimation of the in situ uncertainty of key parameters

It is a difficult task to estimate the real uncertainty of model parameters. For each parameter or variable selected as described above, we have estimated an in situ error. For this purpose, measurements collected on the Hesse site (or on other beech forests near Paris) or data collected from literature have been used. We obtained estimates of input parameters uncertainties based on errors due to ground measurements sampling, instrumentation error, or curve fitting error. In each case a variation coefficient (in percent) was computed. If no measurement error estimation was possible, a variation coefficient of 10% was chosen.

4.3. Evaluation of errors on output variables caused by uncertainty on input parameters

A new set of Monte Carlo simulations was carried out with the uncertainties determined above. This time, the key parameters and variables were all randomly selected with the same procedure described in step (i), except that the standard deviations are not fixed to 10% but correspond to the uncertainty estimated in step (ii). All selected key parameters are processed together to obtain the whole uncertainty on the output variables. This process is repeated many times (e.g. $1000 \times n$, where n is the number of selected key parameters) to generate a wide range of input parameter datasets and to be able to get statistical information on the model outputs. The effect of uncertainties on the key parameters are tested on eight main annual output variables: the net ecosystem exchange (NEE), the gross primary production (GPP), the autotrophic respiration (RA), the heterotrophic respiration (RH), the aerial wood growth (DBwood) in $\mathrm{gC\,m^{-2}\,year^{-1}}$ and the transpiration (Tr) and evapotranspiration (ETR) in $\mathrm{mm\,year^{-1}}$.

The mean and the standard deviation of each annual output variable (NEE, GPP, RA, RH, Tr, ETR) of the $1000 \times n$ runs were calculated, as well as the variation coefficient in percent. The mean daily and standard deviation of NEE were also computed, with the aim to compare them with the daily CO_2 fluxes measured by the eddy covariance technique.

5. Results and discussion

5.1. Determination of key input parameters

Among the 169 parameters and initial conditions, 17 parameters with an effect greater than 2.5% on NEE have been selected as key input parameters (see Table 4). We can distinguish five types of key parameters:

- the dependency between V_{cmax} and leaf nitrogen density, the quantum yield, the ratio between V_{Cmax} and

Table 4
List of key parameters and their effect (max($VR_{+10\%}$,$VR_{-10\%}$)), Eq. (62) and (63) on output variables when a 10% bias is applied on these key parameters

Description	Symbol	NEE	GPP	RH	RA	DBwood	Tr	ETR
Soil volumetric humidity at field capacity	θ_{fcsoil}	23.9	8.5	0.3	2.4	8.6	8.6	4.0
Dependency between V_{cmax} and leaf nitrogen density	α_{Na}	13.5	5.2	0.1	2.4	6.0	4.0	1.8
Soil volumetric humidity at wilting point	$\theta_{wiltsoil}$	12.9	4.6	0.4	1.6	5.9	6.5	3.1
Leaf nitrogen content	$N_{mleaves}$	10.9	5.4	0.1	4.3	4.8	3.6	1.6
Leaf mass per area of sun leaves	LMA_{sunmax}	10.3	5.2	0.2	4.2	5.7	3.4	1.5
Quantum yield	α	10.2	4.0	0.1	1.9	4.7	2.7	1.2
Wood construction cost	CR_{wood}	8.6	0.0	0.0	5.4	4.1	0.0	0.0
Nitrogen dependency for all organs	MRN	8.3	0.2	0.0	5.6	2.8	0.3	0.1
Ratio between VC_{max} and VJ_{max}	β	7.9	3.1	0.1	1.5	3.6	2.1	0.9
Critical value of state of forcing for budburst	F_{critBB}	6.5	3.0	0.2	2.2	3.5	2.2	1.3
Clumping factor	Agreg	5.2	2.0	0.3	0.9	2.3	1.4	0.8
Leaf construction cost	CR_{leaves}	4.1	0.0	0.0	2.6	0.6	0.0	0.0
Critical value of state of forcing for leaf fall	$F_{critLfall}$	3.7	1.5	0.5	0.9	1.4	0.6	0.2
Maximum leaf area index	L_{max}	3.5	2.3	0.8	2.3	2.5	1.9	0.6
Fine roots construction cost	$CR_{fine\ roots}$	3.0	0.0	0.2	2.0	1.6	0.0	0.0
Trunk and branch biomass	Btrunk + Bbranch	3.0	0.0	0.0	1.9	0.8	0.0	0.0
Slope of the ball relationship (maximum value)	g_{1max}	2.6	0.7	0.5	0.1	1.0	7.8	3.6

V_{Jmax}, and the slope of the Ball relationship ($g1_{max}$), which describe the response of photosynthesis and transpiration on meteorological variables and on biochemical parameters.
- the leaf nitrogen content, the maximum sunlit leaf mass per area, the clumping factor and the leaf area index, which represent biochemical and structural input parameters.
- the soil volumetric humidity at field capacity and the soil volumetric humidity at wilting point controlling the extractable water in the soil and therefore the drought effect.
- the fine roots construction cost, the leaves construction cost, the nitrogen dependency for all organs and biomass of trunk and branches allowing the estimation of autotrophic respiration.
- the critical values of state of forcing for budburst and the critical values of state of forcing for leaf fall, which control the phenology.

Among all parameters and initial conditions, only six key parameters have an effect greater than 10% on NEE when they are affected by an Gaussian noise of 10%: soil water content at field capacity, dependency between V_{cmax} and leaf nitrogen density, soil water content at wilting point, leaf nitrogen content, leaf mass per area of sun leaves and the quantum yield.

For an improved sensitivity analysis, it would be interesting to realize this work on several years, to test the possible interannual effects and to have an estimation of the real in situ uncertainty of each parameter. Such a study, coupled with a process uncertainty study would allow us to reduce the number of input parameters and to simplify the model structure.

5.2. Evaluation of the in situ uncertainty of key parameters

The estimated in situ uncertainty (in percent) for the 17 key input parameters are given in Table 5. For four parameters this inference was not achievable. The estimated errors ranged between 3% and 22% with a mean value of 10.2%. The parameters which describe the response of photosynthesis on meteorological variables and on biochemical parameters had a lower uncertainty than the other ones. For 14 key input parameters we were unable to calculate the additional uncertainty due to measurement errors, which was neglected. For this reason the total error is probably underestimated.

The parameters uncertainties are not strictly comparable because they were estimated in different ways: instrumentation error, sampling error (spatial variability) and curve fitting error. Furthermore, different scales and sites are used to assess the spatial variability.

Table 5
Estimation of in situ uncertainty (%) of the key parameters and type of error which are taken into account

	Stand variability	Measurement error	Fit error	Total uncertainty (%)	Sources
θ_{fcsoil}	X			12.1	Granier et al. (2000b)
α_{Na}	X		X	6.1	Liozon et al. (2000)
$\theta_{wiltsoil}$				10.0*	
$N_{mleaves}$	X	X		11	Unpublished data
LMA_{sunmax}	X	X		8.8	Unpublished data
α	X		X	8	Unpublished data
CR_{wood}	X		X	5	Damesin et al. (2002)
MRN			X	10	Ryan (1991)
β	X		X	3	Liozon et al. (2000)
F_{critBB}	X			4.1	Bouriaud (2003)
Agreg	X			14	Soudani personal communication
CR_{leaves}				10.0*	
$F_{critL.fall}$	X			22.2	Bouriaud (2003)
L_{max}	X	X		11	Dufrêne and Bréda (1995)
$CR_{fine\ roots}$				10.0*	
$B_{trunk} + B_{branch}$	X			17.6	Bouriaud (2003)
g_{1max}				10.0*	

* No estimation was available and a mean value of 10% was taken.

5.3. Effect of input parameters uncertainty on output variables

5.3.1. Annual results

The results of the standard simulation and of the ensemble of 17,000 simulations including the 17 key parameters uncertainties are given in Table 6 and Fig. 3. For all output variables except heterotrophic respiration (RH), the mean simulation over 17,000 simulations is smaller than the simulation with the mean input parameters. This result is produced when highly non linear responses $f(x)$ are involved in the model (including threshold effect), and when the current parameter value $\bar{x}$ is close to the threshold. In our case, this effect is not negligible (the difference between $f(\bar{x})$ and $\overline{f(x)}$ reaches 49 gC for the annual

Table 6
Results of annual simulations: reference simulation compared to mean and standard deviation (S.D.) of the 17,000 ensemble simulations including key parameter uncertainties (The percentage uncertainty, or variation coefficient VC is given for the ensemble simulation (mean/S.D.))

Output	Reference simulation	Ensemble mean	Ensemble S.D.	Uncertainty (%)
NEE (gC year^{-1})	463	414	120	29
GPP (gC year^{-1})	1518	1456	151	10
RA (gC year^{-1})	735	722	75	10
RH (gC year^{-1})	321	321	5	2
DBwood (gC year^{-1})	363	348	48	14
ETR (mm year^{-1})	596	590	33	6
Tr (mm year^{-1})	311	302	37	12

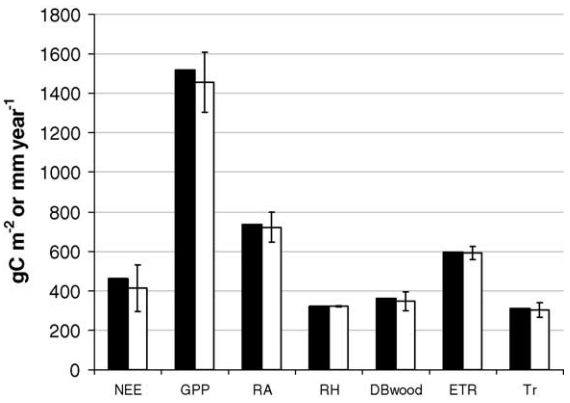

Fig. 3. Annual main output variables (see text for explanation) simulated with mean parameter (black chart). Mean over 15,000 simulations of the same output variables with a random Gaussian noise on key parameters (white chart). The standard deviation used for the random process corresponds to the values reported Table 4. Error bar represents the standard deviation of the output variables. The main output variables chosen are the opposite of net ecosystem exchange (NEE), the gross primary production (GPP), the autotrophic respiration (RA), the heterotrophic respiration (RH), the total wood growth (DB) in gC m^{-2} year^{-1} and the transpiration (Tr) and evapotranspiration (ETR) in mm year^{-1}.

NEE). A detailed study shows that in our case, two parameters are the main cause of the observed difference between $f(\bar{x})$ and $\overline{f(x)}$: θ_{fcsoil} and θ_{wiltsoil}, i.e. the soil volumetric humidities at field capacity and wilting point, both linked to the Soil Extractable Water ($\text{SEW} = \text{RW}_{\text{fc}} - \text{RW}_{\text{wilt}}$). In our case an increase of the SEW above the prescribed value has no effect on the NEE, whereas a decrease in SEW strongly affects NEE. This indicates two things: first, the water stress was moderate in our site during the study (we are near the plateau of $f(x)$: an increase of SEW has little impact on NEE). Second, there is a strong sensitivity to water stress (would there be one): when SEW decreases, NEE largely decreases (i.e. $f(x)$ depends greatly on x). These particular conditions lead to a strong non-linearity around the prescribed value of x, causing a bias in NEE: choosing a mean value for θ_{fcsoil} and θ_{wiltsoil} is not neutral, and the uncertainty in these parameters has to be taken into account in our site and year of study. Generally speaking, this result shows that using the mean value of input parameters instead of explicitly taking into account their spatial variation over the stand leads to significant errors. Therefore, Monte-Carlo approach, in addition to produce estimations of uncertainty in the output variables, corrects the biased results obtained when single values (mean values) of parameters are used, which is almost always the case in current simulation studies.

The output uncertainty is ∼10% on GPP, RV and DB and ∼30% on NEE (see Table 6 and Fig. 3). The large effect on NEE in percent is due to its small value compared to others fluxes and also because NEE was chosen as the key output variable. The standard deviation on NEE corresponds to only 120 gC and cannot fully explain the difference observed between the simulations ($\text{NEE} = 414\ \text{gC m}^{-2}\ \text{year}^{-1}$) and the measurements ($\text{NEE} = 257\ \text{gC m}^{-2}\ \text{year}^{-1}$).

On hydrological output variables the uncertainty is slightly smaller: respectively 6% and ∼12% for ETR and Tr (note, however, that we selected the parameters for their effect on the NEE only).

One must keep in mind that these model uncertainties correspond only to parameters (and initial conditions) errors and do not include the model uncertainty, i.e. uncertainties on processes and modelling errors.

5.3.2. Daily results

The seasonal course of NEE simulation is given in Fig. 4, together with the daily uncertainty estimated using the method described above, and compared to the measurements. The first, logical, observation is that the uncertainty on NEE is greater during the vegetative season. The simulated uncertainty is particularly important at the end of summer (August and September), when a drought occurred. The uncertainty due to errors in leaf fall simulation is also observed in October.

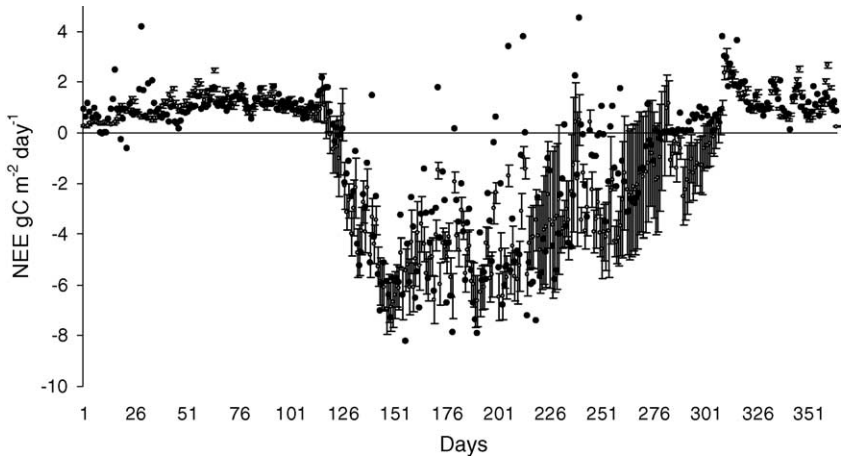

Fig. 4. Daily NEE measured by eddy covariance technique (black circle) and simulated (white circle). Simulations data corresponds to the mean over 15,000 simulations with a yearly random Gaussian noise on key parameters and the error bar is the standard deviation. Here a net input of carbon to the atmosphere is positive.

One notes that the parameterization uncertainty could explain a part of the difference between eddy-covariance measurements and simulations during the winter and the beginning of the leafy season. However, during summer, even if we take into account the uncertainty on simulations, the model seems not to be able to assess the extreme values of measured NEE. On the other hand, the decrease of NEE measured late in summer is fairly reproduced by the model, except in October. This NEE decline might be caused by a delayed action of the summer drought or by a decrease in photosynthetic capacities, which was not taken into account by the model (Wilson et al., 2000).

6. Conclusion

A model simulating the carbon and the water budget at stand scale has been developed. In this study, attention was paid to obtain a precise model parameterization. A comparison with independent fluxes data measured by eddy covariance allows an accurate validation of the model in the Hesse Euroflux site. An overestimation of the simulated NEE was observed and different leads could be investigated to better understand why. The first one is to evaluate the effect of the real uncertainties on key input parameters on the simulated NEE. Seventeen key input parameters lead to an uncertainty of 30% on simulated NEE. The mean of 17,000 simulations with input parameters randomly selected around their mean value is smaller than the simulation using the mean input parameters. The proposed procedure to estimate bias, which is due to non linearities in the model, is an important result and should be further studied and taken into account in future works.

Nevertheless, the difference between modelled and measured NEE is not completely explained by the uncertainty on the key input parameters and must be further understood. Two other hypotheses can be put forward to explain the fact that modelled fluxes, including uncertainties, still differ from measurements: either some processes are not correctly described in the model or some discrepancies exist between the scale at which the model is parameterized and the scale at which the model is validated. To study these issues, it is necessary to test the model for each process with independent measurements and to estimate the carbon and the water budget from the organ to the stand scales.

Acknowledgments

We are grateful to the Office National des Forêts (ONF, the French National Office for Forestry) for giving us facilities for in situ measurements. Financial support was provided by the European community through the Euroflux program (contract ENV4-CT95-0078 and CarboEurope-IP). The author acknowledge Bernard Saugier and Franz Badeck for valuable discussions and J.Y Pontailler for his comments. The authors thanks the anonymous reviewers for their constructive remarks that significantly helped strengthen the paper

Appendix A. Radiative balance in the thermal infrared

In the thermal infrared (TIR) the radiative balance coefficients are based on the general formalism given in François (2002) (hereafter referred to as FR02). The soil–vegetation radiative balance coefficients are written according to MOD3 multiple scattering parameterization (Eqs. (11), (14), (16) and (17) in FR02) adapted for diffuse radiation. These coefficients are τ_v, ρ_v (resp. canopy simple transmittance, reflectance and emissivity), τ_t, ρ_t, (resp. multiple scattering canopy transmittance and reflectance), and ω_t and ε_t (resp. multiple scattering vegetation emissivity/absorbance and canopy emissivity/absorbance). Using these coefficients, the radiative transfer balance for the vegetation and the soil writes:

$$\mathrm{Rn_{veg}} = \varepsilon_t \mathrm{Ra} - (\omega_t + \varepsilon_g\varepsilon_t)\mathrm{Rv} + \varepsilon_g\varepsilon_t \mathrm{Rg}$$

$$\mathrm{Rn_{soil}} = \tau_v\varepsilon_g \mathrm{Ra} - \varepsilon_g(\tau_t + \varepsilon_t)\mathrm{Rg} + \varepsilon_g\varepsilon_t \mathrm{Rv}$$

where $\mathrm{Rn_{veg}}$ (resp. $\mathrm{Rn_{soil}}$) are the net vegetation (resp. soil) absorbed TIR radiation, Rv (resp. Rg) are the blackbody TIR radiation emitted by the leaves (resp. the soil) and Ra the incident TIR atmospheric radiance. Ra is computed according to Iziomon et al. (2003), including a dependence on the cloud cover. Rg and Rv are computed according to Stefan equation using the soil and leaf temperatures. The soil and leaf emissivity are assumed to be constant, equal to 0.97.

The simple and mutiple scattering coefficients τ_v, ρ_v, τ_t, ρ_t, ω_t and ε_t are given by: $\tau_v = 1 - \sigma_f$, where the hemispherical shielding factor (or interception coefficient) σ_f is computed according to Goudriaan (1977).

$$\rho_v = \sigma_f(1 - \varepsilon_v),$$

where ε_v is the leaf emissivity.

$$\tau_t = \frac{\tau_v}{1-(1-\varepsilon_g)\rho_v}$$

where ε_g is the soil emissivity

$$\rho_t = \rho_v + \frac{(1-\varepsilon_g){\tau_v}^2}{1-(1-\varepsilon_g)\rho_v}$$

$$\varepsilon_t = \frac{(1-\rho_v)}{[1-(1-\varepsilon_g)\rho_v]}$$

These formulations are the adaptation for diffuse radiation of Eqs. (11), (14), (16) and (17) published in FR02.

Appendix B. Multi-layer radiative balance in the PAR and the NIR

In CASTANEA the radiative balances in the PAR and NIR are performed through a multi-layer parameterization to account for the vertical distribution of absorbed radiation into the canopy. A forest with LAI = 6 is typically divided into 30 elementary layers.

The SAIL model is used to compute the five elementary reflectances (ρ) and transmittances (τ) for a single elementary layer k: ρ_{dd}, ρ_{sd}, τ_{dd}, τ_{sd}, τ_{ss} (where the subscript s stands for direct radiation and d for diffuse radiation). The input data for the SAIL model are the leaf reflectance and transmittance in the PAR (ρ_{PAR} and τ_{PAR}), the Leaf Inclination Distribution Function (LIDF), the sun elevation and the thickness of the elementary vegetation layer Δ (in LAI units).

Then, for each layer k, the corresponding multiple scattering reflectances (R) and transmittances (T) for layer k, R^k_{dd}, R^k_{sd}, T^k_{ss}, T^k_{dd}, T^k_{sd} are computed:

$$T^k_{ss} = \tau_{ss}$$

$$T^k_{dd} = \frac{\tau_{dd}}{(1-R^{k-1}_{dd}\rho_{dd})(1-\rho_{dd}R^{k+1}_{bot\,dd})(1-R^{k+1}_{bot\,dd}\tau_{dd}R^{k-1}_{dd}\tau_{dd})}$$

$$T^k_{sd} = \frac{\tau_{sd}}{(1-R^{k-1}_{dd}\rho_{dd})} + \frac{\tau_{sd}R^{k+1}_{bot\,dd}\tau_{dd}R^{k-1}_{dd}\tau_{dd}}{(1-R^{k-1}_{dd}\rho_{dd})(1-\rho_{dd}R^{k+1}_{bot\,dd})(1-R^{k+1}_{bot\,dd}\tau_{dd}R^{k-1}_{dd}\tau_{dd})} + \frac{\tau_{ss}R^{k-1}_{sd}\rho_{dd}}{(1-R^{k-1}_{dd}\rho_{dd})} + \frac{\rho_{sd}R^{k+1}_{bot\,dd}\tau_{dd}}{(1-R^{k-1}_{dd}\rho_{dd})(1-\rho_{dd}R^{k+1}_{bot\,dd})(1-R^{k+1}_{bot\,dd}\tau_{dd}R^{k-1}_{dd}\tau_{dd})} + \frac{\tau_{ss}R^{k-1}_{sd}\rho_{dd}R^{k+1}_{bot\,dd}\tau_{dd}R^{k-1}_{dd}\tau_{dd}}{(1-R^{k-1}_{dd}\rho_{dd})(1-\rho_{dd}R^{k+1}_{bot\,dd})(1-R^{k+1}_{bot\,dd}\tau_{dd}R^{k-1}_{dd}\tau_{dd})}$$

$$R^k_{dd} = \frac{\rho_{dd}}{(1-\rho_{dd}R^{k+1}_{bot\,dd})(1-R^{k+1}_{bot\,dd}\tau_{dd}R^{k-1}_{dd}\tau_{dd})}$$

$$R^k_{sd} = \frac{\rho_{sd}}{(1-\rho_{dd}R^{k+1}_{bot\,dd})} + \frac{\rho_{sd}R^{k+1}_{bot\,dd}\tau_{dd}R^{k-1}_{dd}\tau_{dd}}{(1-R^{k-1}_{dd}\rho_{dd})(1-\rho_{dd}R^{k+1}_{bot\,dd})(1-R^{k+1}_{bot\,dd}\tau_{dd}R^{k-1}_{dd}\tau_{dd})}$$

$$R^k_{bot\,dd} = \frac{\rho_{dd}}{(1-R^{k-1}_{dd}\rho_{dd})(1-R^{k+1}_{bot\,dd}\tau_{dd}R^{k-1}_{dd}\tau_{dd})}$$

$$T^k_{bot\,dd} = T^k_{dd}$$

R_{bot} and T_{bot} correspond to reflectances and transmittances involving the bottom of layer k (concerning upcoming radiation, instead of descending radiation).

R^k_{dd}, R^k_{sd}, T^k_{ss}, T^k_{dd} and T^k_{sd} include multiple scattering with the lower $(k-1)$ and upper $(k+1)$ layer. The calculation of T_{dd}, T_{sd}, R_{dd}, R_{sd}, R_{botdd} and T_{botdd} are recursive (the calculations are done for the top layer first, then the second layer, etc., down to the soil layer, and then again). They generally converge after five iterations (five iterations are performed in the model). The subsequent iterations provide only negligible corrections. Note that the multiple reflections are taken into account to infinite order through the denominators. Iterations are required only because of the $(k-1)$ reflectances and transmittances that appear in the equations (coefficients concerning the lower layer) and which are still unknown when coefficient for layer k are computed. They are initialized to their non multiple scattering value, ρ_{dd}, ρ_{sd}, τ_{dd}, τ_{sd}, and τ_{ss}, respectively, for the first iteration.

The details for the four terms of multiple scattering R_{sd} (direct incident radiation reflected to diffuse radiation) are given here for illustration:

$$\frac{\rho_{sd}}{(1-\rho_{dd}R_{bot\,dd}^{k+1})}$$

Single reflection. Subsequent multiple scattering between the top of layer k and the bottom of the upper layer $k+1$ are taken into account through the denominator.

$$\frac{\rho_{sd}R_{bot\,dd}^{k+1}\tau_{dd}R_{dd}^{k-1}\tau_{dd}}{(1-R_{dd}^{k-1}\rho_{dd})(1-\rho_{dd}R_{bot\,dd}^{k+1})(1-R_{bot\,dd}^{k+1}\tau_{dd}R_{dd}^{k-1}\tau_{dd})}$$

The direct incident radiation if first reflected and scattered on the top of layer k, then on the bottom of the upper layer $(k+1)$, then transmitted through layer k down to layer $(k-1)$, reflected on the top of layer $(k-1)$ and transmitted again upwards through layer k. Subsequent multiple scattering are taken into account through the denominator following three possibilities (more reflections between the top of layer $(k-1)$ and the bottom of layer k, more reflections between the bottom of the layer $(k+1)$ and the top of layer k, more reflections between the bottom of the layer $(k+1)$ and the top of layer $(k-1)$ through layer k).

In this example all possibilities are taken into account for a direct incident radiation to be reflected and scattered into diffuse radiation by layer k, including all multiple scattering with layers $(k+1)$ and $(k-1)$: this is the definition of R_{sd}.

The calculations of T_{dd}, T_{sd}, R_{dd}, R_{sd}, R_{botdd} and T_{botdd} follow the same pattern and may be easily reconstructed following the same approach.

We are then able to compute the incident direct I_s^k and diffuse I_d^k radiation above layer k:

$$I_s^k = T_{ss}^{k+1}I_s^{k+1}$$

$$I_d^k = T_{sd}^{k+1}I_s^{k+1} + T_{dd}^{k+1}I_d^{k+1}$$

Knowing the incident direct and diffuse radiation I_s and I_d above layer k, we have to compute the incoming coefficients ($Intop_{dd}$, $Inbottom_{dd}$, $Intop_{sd}$, $Inbottoms_{dd}$) to obtain the incoming diffuse and direct radiation at each layer k (the incoming radiation takes into account the multiple scattering).

Then, using the layer absorption coefficients a_s and a_d, for diffuse and direct radiation respectively, we can compute the direct $aPAR_s^k$ and diffuse $aPAR_d^k$ absorbed radiation by layer k:

$$aPAR_s^k = a_s I_s(K)$$

$$aPAR_d^k = a_d[(Intop_{dd}^k + Inbottom_{dd}^k)I_d(k)Intop_{sd}^k + Inbottom_{sd}^k)I_s(k)]$$

The absorption coefficients a_d and a_s for each layer are:

$$a_d = 1 - \rho_{dd} - \tau_{dd}$$

$$a_s = 1 - \tau_{ss} - \rho_{sd} - \tau_{sd}$$

The incoming coefficients ($Intop_{dd}$, $Inbottom_{dd}$, $Intop_{sd}$, $Inbottom_{sd}$) are computed as follows:

$$Intop_{dd}^k = \frac{1}{(1-\rho_{dd}R_{bot\,dd}^{k+1})} + \frac{R_{bot\,dd}^{k+1}\tau_{dd}R_{dd}^{k-1}\tau_{dd}}{(1-R_{dd}^{k-1}\rho_{dd})(1-\rho_{dd}R_{bot\,dd}^{k+1})(1-R_{bot\,dd}^{k+1}\tau_{dd}R_{dd}^{k-1}\tau_{dd})}$$

$$Intop_{sd}^k = \frac{\rho_{sd}R_{bot\,dd}^{k+1}}{(1-\rho_{dd}R_{bot\,dd}^{k+1})} + \frac{\rho_{sd}R_{bot\,dd}^{k+1}R_{bot\,dd}^{k+1}\tau_{dd}R_{dd}^{k-1}\tau_{dd}}{(1-R_{dd}^{k-1}\rho_{dd})(1-\rho_{dd}R_{bot\,dd}^{k+1})(1-R_{bot\,dd}^{k+1}\tau_{dd}R_{dd}^{k-1}\tau_{dd})} + \frac{\tau_{sd}R_{dd}^{k-1}\tau_{dd}R_{bot\,dd}^{k+1}}{(1-R_{dd}^{k-1}\rho_{dd})(1-\rho_{dd}R_{bot\,dd}^{k+1})(1-R_{bot\,dd}^{k+1}\tau_{dd}R_{dd}^{k-1}\tau_{dd})}$$

$$\mathrm{Inbottom}^k_{\mathrm{dd}} = \frac{\tau_{\mathrm{dd}} R^{k-1}_{\mathrm{dd}}}{(1 - R^{k-1}_{\mathrm{dd}}\rho_{\mathrm{dd}})(1 - \rho_{\mathrm{dd}} R^{k+1}_{\mathrm{bot\,dd}})(1 - R^{k+1}_{\mathrm{bot\,dd}}\tau_{\mathrm{dd}} R^{k-1}_{\mathrm{dd}}\tau_{\mathrm{dd}})}$$

$$\begin{aligned}\mathrm{Inbottom}^k_{\mathrm{sd}} &= \frac{\tau_{\mathrm{sd}} R^{k-1}_{\mathrm{dd}}}{(1 - R^{k-1}_{\mathrm{dd}}\rho_{\mathrm{dd}})} \\ &+ \frac{\tau_{\mathrm{sd}} R^{k+1}_{\mathrm{bot\,dd}}\tau_{\mathrm{dd}} R^{k-1}_{\mathrm{dd}}\tau_{\mathrm{dd}}}{(1 - R^{k-1}_{\mathrm{dd}}\rho_{\mathrm{dd}})(1 - \rho_{\mathrm{dd}} R^{k+1}_{\mathrm{bot\,dd}})(1 - R^{k+1}_{\mathrm{bot\,dd}}\tau_{\mathrm{dd}} R^{k-1}_{\mathrm{dd}}\tau_{\mathrm{dd}})} \\ &+ \frac{\rho_{\mathrm{sd}} R^{k+1}_{\mathrm{bot\,dd}}\tau_{\mathrm{dd}} R^{k-1}_{\mathrm{dd}}}{(1 - R^{k-1}_{\mathrm{dd}}\rho_{\mathrm{dd}})(1 - \rho_{\mathrm{dd}} R^{k+1}_{\mathrm{bot\,dd}})(1 - R^{k+1}_{\mathrm{bot\,dd}}\tau_{\mathrm{dd}} R^{k-1}_{\mathrm{dd}}\tau_{\mathrm{dd}})}\end{aligned}$$

The approach is very similar to the one that allowed the calculation of R^k_{dd}, R^k_{sd}, T^k_{ss}, T^k_{dd}, T^k_{sd}. The difference, since all R^k_{dd}, R^k_{sd}, T^k_{ss}, T^k_{dd}, T^k_{sd} are known, is that iterations are not required any more. For instance, $\mathrm{Intop}_{\mathrm{dd}}$ is the a factor (greater than 1) indicating that incident diffuse radiation on top of layer k is greater than I_{dd} because of multiple scattering with the bottom of upper layer $(k+1)$ (first term) and multiple scattering, through layer k, with the top of layer $(k-1)$ (second term).

$\mathrm{aPAR}^k_{\mathrm{s}}$ and $\mathrm{aPAR}^k_{\mathrm{d}}$ are then used to compute the radiation absorbed by the sunlit and shaded leaves, $\mathrm{aPAR}^k_{\mathrm{sunlit}}$ and $\mathrm{aPAR}^k_{\mathrm{shade}}$, through:

$$\mathrm{aPAR}^k_{\mathrm{sunlit}} = \frac{\mathrm{aPAR}^k_{\mathrm{s}}}{\Delta \cdot p^k_{\mathrm{sun}}} + \frac{\mathrm{aPAR}^k_{\mathrm{d}}}{\Delta}$$

$$\mathrm{aPAR}^k_{\mathrm{shade}} = \frac{\mathrm{aPAR}^k_{\mathrm{d}}}{\Delta}$$

Δ is the layer thickness (in LAI units) and p^k_{sun} the mean proportion of sunlit leaves in layer k:

$$p^k_{\mathrm{sun}} = \frac{\mathrm{TT}^{k+1}_{\mathrm{ss}} + \mathrm{TT}^k_{\mathrm{ss}}}{2}$$

where $\mathrm{TT}^k_{\mathrm{ss}}$ is the total transmittance for the direct radiation at layer k:

$$\mathrm{TT}^k_{\mathrm{ss}} = (T^k_{\mathrm{ss}})^{n_{\mathrm{layer}}+1-k}$$

n_{layer} is the total number of layers, about 30 in the model.

$\mathrm{aPAR}^k_{\mathrm{sunlit}}$ and $\mathrm{aPAR}^k_{\mathrm{shade}}$ are the quantities that finally enter the photosynthesis module.

Note: the direct radiation $\mathrm{aPAR}^k_{\mathrm{s}}/\Delta \cdot p^k_{\mathrm{sun}}$ absorbed by the sunlit leaves is in fact constant and equal to:

$$\frac{\mathrm{aPAR}^k_{\mathrm{s}}}{\Delta \cdot p^k_{\mathrm{sun}}} = \frac{a_{\mathrm{s}}}{(\Delta \cdot (1 + \tau_{\mathrm{ss}}))/2} I^{\mathrm{PAR}}_{\mathrm{s0}}$$

where $I^{\mathrm{PAR}}_{\mathrm{s0}}$ is the incident direct radiation in the PAR.

Furthermore the factor $(a_{\mathrm{s}})/(\Delta(1+\tau_{\mathrm{ss}})/2)$ is in fact independent of LAI and layer thickness Δ, and only depends on leaf reflectance ρ_{PAR}, leaf transmittance τ_{PAR} and LIDF.

References

Aber, J.D., Federer, A., 1992. A generalized, lumped-parameter model of photosynthesis, evapotranspiration and net primary production in temperate and boreal forest ecosystems. Oecologia 92, 463–474.

Ågren, G.I., Axelsson, B., 1980. A tree growth model. In: Persson, T. (Ed.), Structure and function of Northern coniferous forests, an ecosystem study. Ecol. Bull., Stockholm, pp. 525–536.

Amthor, J.S., 1994. Scaling CO_2-photosynthesis relationships from the leaf to the canopy. Photosynth. Res. 39, 321–350.

Aussenac, G., Ducrey, M., 1977. Etude bioclimatologique d'une futaie de feuillus (*Fagus sylvatica* L. et *Quercus sessiliflora* Salisb.) de l'Est de la France. I. Analyse des profils microclimatiques et des caractéristiques anatomiques et morphologiques de l'appareil foliaire. Ann. Sci. For. 34 (4), 265–284.

Baldocchi, D.D., 1992. A Lagrangian random walk model for simulating water vapour, CO_2, and sensible heat flux densities and scalar profiles over and within a soybean canopy. Bound. Layer Meteorol. 61, 113–144.

Baldocchi, D.D., 1994. An analytical solution for coupled leaf photosynthesis and stomatal conductance models. Tree Physiol. 14, 1069–1079.

Baldocchi, D.D., Harley, P.C., 1995. Scaling carbon dioxide and water vapour exchange from leaf to canopy in a deciduous forest.

II. Model testing and application. Plant Cell. Environ. 18 (10), 1157–1173.

Ball, J.T., Woodrow, I.E., Berry, J.A., 1987. A model predicting stomatal conductance and its contribution to the control of photosynthetis under different environmental conditions. In: Biggins, J. (Ed.), Progress in Photosynthesis Research, vol. 4, pp. 221–224.

Barbaroux, C., 2002. Analyse et modélisation des flux de carbone de peuplements forestiers pour la compréhension de la croissance des espèces feuillues Quercus petraea et Fagus sylvatica. Ph.D. thesis, Univ. Paris XI (Orsay), 183p.

Barbaroux, C., Bréda, N., Dufrêne, E., 2003. Distribution of aboveground and belowground carbohydrate reserves in adult trees of two contrasting broad-leaved species (*Quercus petraea* and *Fagus sylvatica*). New Phytol. 157, 605–615.

Bauhus, J., Bartsch, N., 1996. Fine-root growth in beech (*Fagus sylvatica*) forest gaps. Can. J. For. Res. 26, 2153–2159.

Becker, M., Nieminen, T.M., Gérémia, F., 1994. Short-term variations and long term changes in oak productivity in northeastern France. The role of climate and atmospheric CO_2. Ann. Sci. For. 51, 477–492.

Bernacchi, C.J., Singsaas, E.L., Pimentel, C., Portis, A.R., Long, S.P., 2001. Improved temperature response functions for models of Rubisco-limited photosynthesis. Plant Cell. Environ. 24, 253–259.

Black, T.A., 1979. Evapotranspiration from Douglas firs stands exposed to soil water deficits. Water Resour. Res. 15 (1), 164–170.

Bossel, H., 1996. TREEDYN3 forest simulation model. Ecol. Model 90, 187–227.

Boulet, G., Chechbouni, A., Braud, I., Vauclin, M., Haverkamp, R., Zammint, C., 2000. A simple water and enrgy balance model designed for regionalization and remote sensing data utilization. Agric. For. Meteorol. 105, 117–132.

Bouriaud, O., 2003. Analyse fonctionnelle de la productivité du hêtre: influences des conditions du milieu, de la structure du peuplement et du couvert, effets de l'éclaircie. PhD-Thèse de l'ENGREF et INRA, Nançy, France, 285p.

Braud, I., Dantas-Antonino, A.C., Vauclin, M., Thony, J.L., Ruelle, P., 1995. A simple soil-plant atmosphere transfer model (SiSPAT) development and field verification. J. Hydrol. 166, 213–250.

Brooks, A., Farquhar, G.D., 1985. Effect of temperature on the CO_2/O_2 specificity of ribulose-1,5-bisphosphate carboxylase\oxygénase and the rate of respiration in the light. Estimates from gas-exchange measurements on spinach. Planta 165, 397–406.

Caldwell, M.M., Meister, H.P., Tenhunen, J.D., Lange, O.L., 1986. Canopy structure, light microclimate and leaf gas exchange of *Quercus coccifera* L. in a Portuguese macchia: measurements in different canopy layers and simulations with a canopy model. Trees 1, 25–41.

Campbell, G.S., 1986. Extinction coefficients for radiation in plant canopies calculated using an ellipsoidal inclination angle distribution. Agric. For. Meteorol. 36, 317–321.

Cannell, M.G.R., Sheppard, L.J., Milne, R., 1988. Light use efficiency and woody biomass production of poplar and willow. Forestry 61, 125–136.

Ceschia, E., Damesin, C., Lebaube, S., Pontailler, J.-Y., Dufrêne, E., 2002. Spatial and seasonal variations in stem respiration of beech trees (*Fagus sylvatica*). Ann. For. Sci. 59, 801–812.

Chassagneux, P., Choisnel, E., 1986. Modélisation de l'évaporation globale d'un couvert forestier. I. Principes physiques et description du modèle. Ann. Sci. For. 43 (4), 505–520.

Chassagneux, P., Choisnel, E., 1987. Modélisation de l'évaporation globale d'un couvert forestier. II. Calibrages et résultats du modèle. Ann. Sci. For. 44 (2), 171–188.

Chen, H., Harmon, M.E., Sexton, J., Fasth, B., 2002. Fine-root decomposition and N dynamics in coniferous forests of the Pacific Northwest. USA. Can. J. For. Res. 32 (3), 20–331.

Collatz, G.J., Ball, J.T., Grivet, C., Berry, J.A., 1991. Physiological and environmental regulation of stomatal conductance, photosynthesis and transpiration: a model that includes a laminar boundary layer. Agric. For. Meteorol 54 (2–4), 107–136.

Damesin, C., Ceschia, E., Le Goff, N., Ottorini, J.M., Dufrêne, E., 2002. Stem and branch respiration of beech: from tree measurements to estimations at the stand level. New Phytol. 153, 159–172.

Davi, H., 2004. Développement d'un modèle générique simulant les flux et les stocks de carbone et d'eau dans le cadre des changements climatiques. Thèse de Doct. en Sci., Univ. Paris-Sud, Orsay, 213 p. + annexes.

De Pury, D.G.G., Farquhar, G.D., 1997. Simple scaling of photosynthesis from leaves to canopies without the errors of big-leaf models. Plant, Cell Environ. 20, 537–557.

Dhôte, J.F., 1990. Modèles de la dynamique des peuplements forestiers: articulation entre les niveaux de l'arbre et du peuplement. Application à la sylviculture des hêtraies. Thèse de l'Université Claude Bernard Lyon I, 240 p. + annexes.

Dhôte, J.F., 1991. Modélisation de la croissance des peuplements réguliers de hêtre: dynamique des hiérarchies sociales et facteurs de production. Ann. Sci. For. 48, 389–416.

Dhôte, J.F., Hervé, J.C., 2000. Changements de productivité dans quatre forêts de chêne sessiles depuis 1930: une approche au niveau du peuplement. Ann. Sci. For. 57, 651–680.

Dommergues, S.Y., Mangenot, F., 1970. Écologie Microbienne du sol.. Masson & Cie, Paris, 796 p.

Ducrey, M., 1981. Etude bioclimatologique d'une futaie de feuillus (*Fagus sylvatica* L. et *Quercus sessiliflora* Salisb.) de l'Est de la France. III. Potentialités photosynthétiques à différentes hauteurs dans le peuplement. Ann. Sci. For. 38 (1), 71–86.

Dufrêne, E., 1989. Photosynthèse. In: consommation en eau et modélisation de la production chez le palmier à huile (Elaeis guineensis Jacq.). Thèse de Doctorat, Université d'Orsay, France, 157p.

Dufrêne, E., Dubos, B., Rey, H., Quencez, P., Saugier, B., 1992. Changes in evapotranspiration from oil palm stand (*Elaeis guineensis* Jacq.) exposed to seasonal water deficits. Act. Oecol. 13 (3), 299–314.

Dufrêne, E., Bréda, N., 1995. Estimation of deciduous forest leaf area index using direct and indirect methods. Oecologia, 156–162.

Eagleson, P.S., 1978. Climate, soil and vegetation 3. A simplified model of soil moisture movment in the liquid phase. Water Resour. Res. 14 (5), 713–721.

Ehleringer, J., Björkman, O., 1977. Quantum yields for CO_2 uptake in C_3 and C_4 plants. Dependence on temperature, CO_2 and O_2 concentration. Plant Physiol. 59, 86–90.

Elzein, A., Balesdent, J., 1995. Mechanistics simulation of vertical distribution of carbon concentrations and residence times in soils. Soil Sci. Soc. Am. Jour. 59, 1328–1335.

Epron, D., Badot, P.M., 1997. Fine root respiration in forest trees. In: Puech, J.C., Latché, A., Bouzyen, M. (Eds.), Plant Sciences 1997. Société Française de Physiologie Végétale, Paris, pp. 199–200.

Epron, D., Le Dantec, V., Dufrêne, E., Granier, A., 2001. Seasonal dynamics of soil carbon efflux and simulated rhizosphere respiration in a beech forest. Tree Physiol. 21, 145–152.

Farque, L., 1997. Contribution des racines de hêtre (Fagus sylvatica L.) au bilan carboné d'un sol forestier. DEA d'Ecologie, Université Paris XI, Orsay, 28 p.

Farquhar, G.D., von Caemmerer, S., Berry, J.A., 1980. A biochemical model of photosynthetic CO_2 assimilation in leaves of C_3 species. Planta 149, 78–80.

François, C., 2002. The potential of directional radiometric temperatures for monitoring soil and leaf temperatures and soil moisture status. Remote Sens. Environ. 80 (1), 122–133.

Franks, S.W., Beven, K.J., 1997. Bayesian estimation of uncertainty in land surface – atmosphere flux predictions. J. Geophys. Res. 102 (D20), 23991–23999.

Franks, S.W., Beven, K.J., Gash, J.H.C., 1999. Multi-objective conditioning of a simple SVAT model. Hydrol. Earth System Sci. 3 (4), 477–489.

Goudriaan, J., 1977. Crop micrometeorology: a simulation study. Simulation Monographs. Pudoc, Wageningen. 257 p.

Granier, A., Bréda, N., Biron, P., Villette, S., 1999. A lumped water balance model to evaluate duration and intensity of drought constraints in forest stands. Ecol. Model. 116, 269–283.

Granier, A., Ceschia, E., Damesin, C., Dufrêne, E., Epron, D., Gross, P., Lebaube, S., Le Dantec, V., Le Goff, N., Lemoine, D., Lucot, E., Ottorini, J.M., Pontailler, J.Y., Saugier, B., 2000a. The carbon balance of a young beech forest. Funct. Ecol. 14, 312–325.

Granier, A., Biron, P., Lemoine, D., 2000b. Water balance, transpiration and canopy conductance in two beech stands. Agric. For. Meteorol. 100, 291–308.

Haan, C.T., Storm, D.E., Al-Issa, T., Prabhu, S., Sabbagh, G.J., Edwards, D.R., 1998. Effect of parameter distributions on uncertainty analysis of hydrologic models. Trans ASAE 41 (1), 65–70.

Helvey, J.D., Patric, J.H., 1965. Canopy and litter interception of rainfall by hardwoods of eastern United States. Water Resour. Res. 1, 193–206.

Hoffmann, F., 1995. FAGUS, a model for growth and development of beech. Ecol. Model. 83, 327–348.

Idso, S.B., 1981. A set of equations for full spectrum and 8 to 14 μm and 10.5 to 12.5 μm thermal radiation from cloudless skies. Water Resour. Res. 17 (2), 295–304.

Iziomon, M.G., Mayer, H., Matzarakis, A., 2003. Downward atmospheric longwave irradiance under clear and cloudy skies: measurement and parameterization. J. Atm. Solar-Terrestrial Phys. 65 (10), 1107–1116.

Jackson, R.B., Mooney, H.A., Schulze, E.D., 1997. A global buget for fine root biomass, surface area, and nutrient contents. Proc. Natl. Acad. Sci. U.S.A. 94, 7362–7366.

Jarvis, P.G., 1976. The interpretation of the variations in leaf water potential and stomatal conductance found in canopies in the field. Ph. Trans. R. Soc. Lond. Ser. B 273, 593–610.

Käärik, A.A., 1974. Decomposition of wood. In: Dickinson, C.H., Pugh, G.J.F. (Eds.), Biology of Plant Litter Decomposition, vol. I. Academic Press, London, pp. 129–174.

Kelliher, F.M., Black, T.A., Price, D.T., 1986. Estimating the effects of understorey removal from Douglas fir forest using a two-layer canopy evapotranspiration model. Water Resour. Res. 22, 1891–1899.

Kirschbaum, M.U.F., Farquhar, G.D., 1984. Temperature dependence of whole-leaf photosynthesis in Eucalyptus pauciflora Sieb. ex Spreng. Australian Journal of Plant Physiol. 11, 519–538.

Kirschbaum, M.U.F., Farquhar, G.D., 1987. Investigation of the CO_2 dependance of quantum yield and respiration in *Eucalyptus pauciflora*. Plant. Physiol. 83, 1032–1036.

Korol, R.L., Running, S.W., Milner, K.S., Hunt, E.R., 1991. Testing a mechanistic carbon balance model against observed tree growth. Can. J. For. Res. 21, 1098–1105.

Kramer, K., 1994. Selecting a model to predict the onset of growth of *Fagus sylvatica*. J. Appl. Ecol. 31, 172–181.

Lafleur, P.M., Rouse, W.R., 1989. Application of an energy combination model for evaporation from sparse canopies. Agric. For. Meteorol. 49, 135–153.

Le Dantec, V., 2000. Modélisation des échanges carbonés et hydriques dans un écosystème forestier: un modèle couplé sol-plante. Thèse Université, Paris XI.

Le Dantec, V., Dufrêne, E., Saugier, B., 2000. Interannual and spatial variation in maximum leaf area index of temperate deciduous stands. For. Ecol. Manage. 134, 71–81.

Le Goff, N., Ottorini, J.-M., 2001. Root biomass and biomass increment in a beech (*Fagus sylvatica* L.) stand in North-East France. Ann. For. Sci. 58, 1–13.

Leuning, R., Kelliher, F.M., de Pury, D.G.G., Schulze, E.D., 1995. Leaf nitrogen, photosynthesis, conductance and transpiration: scaling from leaves to canopy. Plant Cell Environ. 18 (10), 1183–1200.

Leuning, R., Moncrieff, J., 1990. Eddy-covariance CO_2 flux measurements using open-path and close path CO_2 analysers. Corrections for analyser water vapour sensitivity and damping of fluctuations in air sampling tubes. Bound. Layer Meteorol. 53, 63–67.

Leyton, L., Reynolds, E.R.C., Thomson, F.B., 1967. Rainfall interception in forest and moorland. In: Sopper, W.E., Lull, H.W. (Eds.), Forest Hydrology. Pergamon Press, Oxford, pp. 163–178.

Liozon, R., Badeck, F.W., Genty, B., Meyer, S., Saugier, B., 2000. Leaf photosynthetic characteristics of beech (*Fagus sylvatica* L.) saplings during three years of exposure to elevated CO_2 concentration. Tree Physiol. 20, 239–247.

Long, S.P., 1991. Modification of the response of photosynthetic productivity to rising temperature by atmospheric CO_2 concentration: has its importance been underestimated? Plant Cell Environ. 14, 729–739.

Magnani, F., Mencuccini, M., Grace, J., 2000. Age-related decline in stand productivity: the role of structural acclimation under hydraulic constraints. Plant Cell Environ. 23 (251), 263.

Matteucci, G., 1998. Bilancio del carbonio in una faggeta dell'Italia Centro-Meridionale: determinanti ecofisiolo-gici, integrazione a livello di copertura e simulazione dell'impatto dei cambiamenti ambientali. Tesi di dottorato, Università degli studi di Padova. Padova: 227 pp.

McMurtrie, R., Wolf, L., 1983. Above and below ground growth of forest stands: a carbon budget model. Ann. Bot. 52, 449–458.

McMurtrie, R., 1985. In: Cannell, M.G.R., et Jackson, J.E. (Eds.), Forest productivity in relation to carbon partitioning and nutrient cycling: a mathematical model attributes of trees as crop plants. ITE, Monks Wood, Abbots Ripton, Hunts, UK, pp. 194–204.

McMurtrie, R.E., Rook, D.A., Kelliher, F.M., 1990. Modelling the yield of *Pinus radiata* on a site limited by water and nitrogen. For. Ecol. Manage. 30, 381–413.

Medlyn, B.E., Barton, C.V.M., Broadmeadow, M.S.J., Ceulemans, R., De Angelis, P., Forstreuter, M., Freeman, M., Jackson, S.B., Kellomäki, S., Laitat, E., Rey, A., Roberntz, P., Sigurdsson, B.D., Strassemeyer, J., Wang, K., Curtis, P.S., Jarvis, P.G., 2001. Stomatal conductance of forest species after long-term exposure to elevated CO_2 concentration: a synthesis. New Phytol. 149, 247–264.

Mohren, G.M.J., 1987. Simulation of forest growth, applied to Douglas fir stands in the Netherlands. Ph.D. thesis, Wageningen, Netherland, 184 p.

Monteith, J.L., 1965. Evaporation and environment. In: The state and movement of water in living organisms, XIX TII Symposium of the Society for Experimental biology. Cambridge University Press, New York, pp. 205–233.

Nagler, P.L., Daughtry, C.S.T., Goward, S.N., 2000. Plant litter and soil reflectance. Remote Sens. Environ. 71, 207–215.

Niinemets, U., 1999. Energy requirement for foliage formation is not constant along canopy light gradients in temperate deciduous trees. New Phytol. 141, 459–470.

Nizinski, J.J., Saugier, B., 1988. Mesures et modélisation de l'interception nette dans une futaie de chênes. Act. Oecol. Oecol. Planta 9, 311–329.

Nolan, W.G., Smillie, R.M., 1976. Multi-temperature effects on Hill reaction, activity of barley chloroplasts. Biochim. Biophys. Acta 440, 461–475.

Parton, W.J., Schimel, D.S., Cole, C.V., Ojima, D.S., 1987. Analysis of factors controlling soil organic matters levels in great plains grasslands. Soil Sci. Soc. Am. J. 51, 1173–1179.

Penman, H.L., 1948. Natural evaporation from open water, bare soil and grass. Proc. R. Soc. Lond. Ser. A vol. 193, 120–145.

Penning de Vries, F.W.T., 1975a. Use of assimilates in higher plants. In: Photosynthesis, Productivity in different environments, Cooper, J.P. (Eds.), International Biological Programme 3. Cambridge University Press, London, pp. 459–480.

Penning de Vries, F.W.T., 1975b. The cost of maintenance processes in plant cells. Ann. Bot. 39, 77–92.

Penning de Vries, F.W.T., Brunsting, A.H.M., Van Laar, H.H., 1974. Products, requirement and efficiency of biosynthesis: a quantitative approach. J. Theor. Biol. 45, 339–377.

Planchais, I., Pontailler, J.Y., 1999. Validity of leaf areas and angles estimated in a beech forest from analysis of gap frequencies, using hemispherical photographs and a plant canopy analyzer. Ann. For. Sci. 56, 1–10.

Pontailler, J.Y., Genty, B., 1996. A simple red:far-red sensor using gallium arsenide phosphide detectors. Func. Ecol. 10, 535–540.

Quentin, C., Bigorre, F., Granier, A., Bréda, N., Tessier, D., 2001. Etude des sols de la forêt de Hesse (Lorraine) Contribution à l'étude du bilan hydrique. Etude et Gestion des sols 8, 279–292.

Rambal, S., Damesin, C., Joffre, R., Methy, M., Lo Seen, D., 1996. Optimization of carbon gain in canopies of mediterranean evergreen oaks. Ann. For. Sci. 53, 547–560.

Rayner, A.D.M., Boddy, L., 1988. Fungal decomposition of wood: its biology and ecology. John Wiley & Sons, Chichester, 587p.

Ross, D.J., Tate, K.R., Feltham, C.W., 1996. Microbial biomass, and C and N mineralization, in litter and mineral soil of adjacent montane ecosystems in a southern beech (*Nothofagus*) forest and a tussock grassland. Soil Biol. Biochem. 28 (12), 1613–1620.

Running, S.W., Coughlan, J.C., 1988. A general model of forest ecosystem processes for regional applications. I. Hydrologic balance, canopy gas exchange and primary production processes. Ecol. Model. 42, 125–154.

Running, S.W., Hunt, R.E., 1993. Generalization of a forest ecosystem process model for other biomes, BIOME-BGC, and an application for global-scale models. In: Ehleringer, J.R., Field, C.B. (Eds.), Scaling Physiologic Processes: Leaf to Globe. Academic Press, San Diego, CA, pp. 141–158.

Rutter, A.J., Kershaw, K.A., Robins, P.C., Morton, A.J., 1971. A predictive model of rainfall interception in forests. I. Derivation of the model from observations in a plantation of Corsican pine. Agric. Meteorol. 9, 367–384.

Ryan, G.M., 1991. Effects of climate change on plant respiration. Ecol. Appl. 1 (2), 157–167.

Sala, A., Tenhunen, J.D., 1996. Simulations of canopy net photosynthesis and transpiration in Quercus ilex L. under the influence of seasonal drought. Agric. For. Meteorol. 78, 203–222.

Sharp, R.E., Matthews, M.A., Boyer, J.S., 1984. Kok effect and the quantum yield of photosynthesis. Plant Physiol. 75, 95–101.

Schaap, M.G., Bouten, J.M., Verstratent, J.M., 1997. Forest floor water content dynamics in a Douglas fir stand. J. Hydrol. 201, 367–383.

Schober, R., 1975. Ertragstafeln wichtiger Baumarten bei verschiedener Durchforstung. J.D. Sauerländer's Verlag, Frankfurt am Main, 154.

Schulte, M., 1993. Saisonale und interannuelle Variabilität des CO_2-Gaswechsels von Buchen (*Fagus sylvatica* L.). Bestimmung von C-Bilanzen mit Hilfe eines empirischen Modells. Aachen: Shaker Schulze. E. -D. 1970. Der CO_2-Gaswechsel der Buche (*Fagus silvatica* L.) in Abhängigkeit von den Klimafaktoren im Freiland. Flora 159, 177–232.

Schulze, E.D., 1986. Carbon dioxide and water vapour exchange in response to drought in the atmosphere and in the soil. Annu. Rev. Plant Physiol. 37, 247–274.

Shuttleworth, W.J., Wallace, J.S., 1985. Evaporation from sparse crops—an energy combination theory. Q. J. R. Meteorol. Soc. 111, 839–855.

Spear, R.C., Hornberger, G.M., 1980. Eutrophication in Peel Inlet II. Identification of critical uncertainties via generalised sensitivity analysis. Water Res. 14, 43–49.

Spitters, C.J.T., 1986. Separating the diffuse and direct component of global radiation and its implications for modelling canopy

photosynthesis. Part II. Calculation of canopy photosynthesis. Agric. For. Meteorol. 38, 231–242.
Spitters, C.J.T., Toussaint, H.A.J.M., Goudriaan, J., 1986. Separating the diffuse and direct component of global radiation and its implications for modelling canopy photosynthesis. Part I. Components of incoming radiation. Agric. For. Meteorol. 38, 217–229.
Thornley, J.H.M., Johnson, I.R., 1990. Parttionning during vegetative growth. In: Plant and Crop Modelling. Clarendon Press, Oxford (Chapter 13).
Van Bavel, C.H.M., 1966. Potential evaporation: the combination concept and its experimental verification. Water Resour. Res. 2 (3), 455–457.
Van Praag, H.J., Sougnez-Remy, S., Weissen, F., Carletti, G., 1988. Root turnover in a beech and spruce stand of the Belgian Ardennes. Plant Soil 105, 87–103.
Verhoef, W., 1984. Light scattering by leaf layers with application to canopy reflectance modeling: the SAIL model. Remote Sens. Environ. 16, 125–141.
Verhoef, W., 1985. Earth observation modelling based on layer scattering matrices. Remote Sens. Environ. 17, 165–178.
Villar, R., Held, A.A., Merino, J., 1995. Dark leaf respiration in light and darkness of an evergreen and a deciduous plant species. Plant Physiol. 107, 421–427.
Vose, J.M., Bolstad, P.V., 1999. Challenges to modelling NPP in diverse eastern deciduous forests: species-level comparisons of foliar respiration responses to temperature and nitrogen. Ecol. Model. 122, 165–174.
Waelbroeck, C., 1995. Modélisation des échanges de CO2 entre la biosphère et l'atmosphère dans la Toundra. Thèse de doctorat, Université Libre de Bruxelles, Bruxelles, 182 p.
Wang, Y.-P., Leuning, R., 1998. A two-leaf model for canopy conductance, photosynthesis and partitioning of available energy I: model description and comparison with a multi-layered model. Agric. For. Meteorol. 91, 89–111.
Wang, Y.P., Jarvis, P.G., 1990. Influence of crown structural properties on PAR absorption, photosynthesis and transpiration in Sitka spruce: application of a model (MAESTRO). Tree Physiol. 7, 297–316.
Williams, M., Rastetter, E.B., Fernandes, D.N., Goulden, M.L., Wofsy, S.C., Shaver, G.R., 1996. Modelling the soil-plant-atmosphere continuum in a Quercus-Acer stand at Harvard Forest: the regulation of stomatal conductance by light, nitrogen and soil/plant hydraulic properties. Plant Cell. Environ. 19, 911–927.
Wilson, K.B., Baldocchi, D.D., Hanson, P.J., 2000. Spatial and seasonal variability of photosynthetic parameters and their relationship to leaf nitrogen in a deciduous forest. Tree Physiol. 20, 565–578.
Wolters, V., Joergensen, R.G., 1991. Microbial carbon turnover in beech forest soil at different stages of acidification. Soil Biol. Biochem. 23 (9), 897–902.